eNeuro

Research Article: Confirmation

Cognition and Behavior

Intrinsic Excitability in Layer IV–VI Anterior Insula to Basolateral Amygdala Projection Neurons Correlates with the Confidence of Taste Valence Encoding

Sailendrakumar Kolatt Chandran,[1,*] Adonis Yiannakas,[1,3,*] Haneen Kayyal,[1] Randa Salalha,[1] Federica Cruciani,[1] Liron Mizrahi,[1] Mohammad Khamaisy,[1] Shani Stern,[1] and Kobi Rosenblum[1,2]

https://doi.org/10.1523/ENEURO.0302-22.2022

[1]Sagol Department of Neurobiology, University of Haifa, Abba Khoushy Ave 199, Haifa, 3498838, Israel, [2]Center for Gene Manipulation in the Brain, University of Haifa, Haifa, Israel, and [3]Institute of Biochemistry and Molecular Medicine, University of Bern, Bühlstrasse 28, 3012 Bern, Switzerland

Visual Abstract

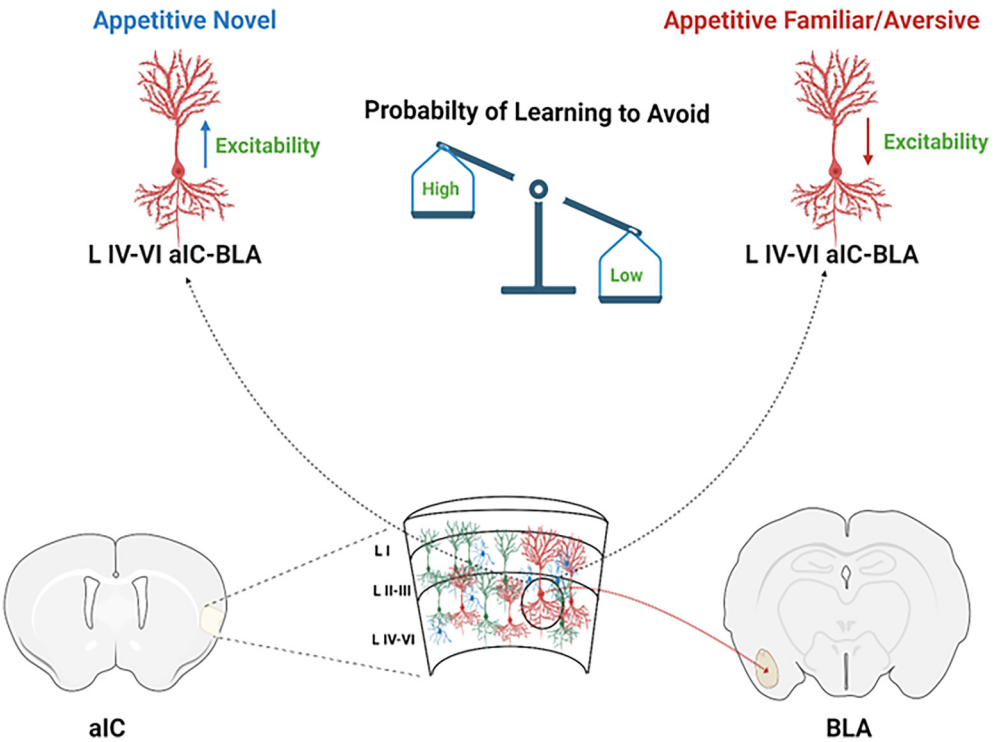

Avoiding potentially harmful, and consuming safe food is crucial for the survival of living organisms. However, the perceived valence of sensory information can change following conflicting experiences. Pleasurability and aversiveness are two crucial parameters defining the perceived valence of a taste and can be impacted by novelty. Importantly, the ability of a given taste to serve as the conditioned stimulus (CS) in conditioned taste aversion (CTA) is dependent on its valence. Activity in anterior insula (aIC) Layer IV–VI pyramidal neurons projecting to the basolateral amygdala (BLA) is correlated with and necessary for CTA learning and retrieval, as well as the expression of neophobia toward novel tastants, but not learning taste familiarity. Yet, the cellular

Significance Statement

Learning to form aversive or safe taste memories is dependent on genetic predisposition as well as previous experiences. In mice, anterior insula (aIC) neurons projecting to the basolateral amygdala (aIC-BLA) are indispensable for learning and retrieving learned taste aversion. Here we demonstrate that the intrinsic properties of aIC-BLA neurons, represent the certainty of taste valence prediction, but not percept. Predictive valence-specific changes are reflected through excitability, being low when taste outcome is highly predictive (i.e., following aversive taste memory retrieval or unreinforced familiarization), and high when taste valence is uncertain (i.e., following novelty or aversive taste memory extinction). In addition, the results propose a neuronal mechanism underlying the long delay between taste and visceral discomfort in conditioned taste aversion (CTA).

mechanisms underlying the updating of taste valence representation in this specific pathway are poorly understood. Here, using retrograde viral tracing and whole-cell patch-clamp electrophysiology in trained mice, we demonstrate that the intrinsic properties of deep-lying Layer IV–VI, but not superficial Layer I–III aIC-BLA neurons, are differentially modulated by both novelty and valence, reflecting the subjective predictability of taste valence arising from prior experience. These correlative changes in the profile of intrinsic properties of LIV–VI aIC-BLA neurons were detectable following both simple taste experiences, as well as following memory retrieval, extinction learning, and reinstatement.

Key words: association; insula; intrinsic properties; novel; salience; taste

Introduction

In the natural setting, animals approach novel taste stimuli tentatively, as to closely examine them according to a genetic plan, as well as in relation to associated visceral consequences (Schier and Spector, 2019). Bitter and sour tastes are innately aversive, acting as warning signals for the presence of toxins (Bachmanov et al., 1996). Conversely, neophobia to innately appetitive sweet and moderately salty tastants dissipates over time (Lin et al., 2012). Importantly, animals can learn to avoid innately appetitive tastants [e.g., saccharin-, or NaCl-water; the conditioned stimulus (CS)], through conditioned taste aversion (CTA; Garcia et al., 1955; Nachman and Ashe, 1973). This single-trial associative learning paradigm results in robust aversion following the pairing of the CS with a malaise-inducing agent [the unconditioned stimulus (US)], such as LiCl (Bures et al., 1998). CTA memories are robust, but can be extinguished through unreinforced CS re-exposures, and subsequently reinstated through US re-exposure (Schachtman et al., 1985; Mickley et al., 2004). Unlike other forms of classical conditioning, the interstimulus interval (ISI) between taste experience (CS) and visceral outcome (US), extends to several hours (Adaikkan and Rosenblum, 2015). How CTA learning enables this long-trace associative process, within timeframes that deviate from classical Hebbian plasticity mechanisms is currently unknown (Chinnakkaruppan et al., 2014; Adaikkan and Rosenblum, 2015).

The primary taste cortex, the anterior insula (aIC), along with the basolateral amygdala (BLA), govern the encoding and retrieval of taste information (Piette et al., 2012; Bales et al., 2015). Gustatory processing in IC neurons encompasses thalamocortical and corticocortical inputs that relay taste-, as well as palatability-related inputs from the BLA, that reflect the emotional valence associated with taste stimuli (Stone et al., 2020). Neuronal taste responses at the IC and BLA are plastic and spatially dispersed, using temporal information to encode multiple types of information relating to stimulus identity and palatability (Grossman et al., 2008; Sadacca et al., 2012; Arieli et al., 2020; Vincis et al., 2020). Both synaptic plasticity and neuronal intrinsic properties are proposed to serve as cellular mechanisms underlying learning and memory (Citri and Malenka, 2008; Sehgal et al., 2013). CTA learning promotes LTP induction in the BLA-IC pathway (Jones et al., 1999; Juárez-Muñoz et al., 2017), and strengthens cell type-specific functional connectivity along the projection (Haley et al., 2016). Intrinsic excitability is the tendency of neurons to fire action potentials (APs) when exposed to inputs, reflecting changes in the suit and properties of specific ion channels (Disterhoft et al., 2004; Song and Moyer, 2018). Although independent mechanisms are involved, recent evidence indicates learning and

Received July 24, 2022; accepted September 11, 2022; First published December 9, 2022.

The authors declare no competing financial interests.

Author contributions: S.K.C., A.Y., and K.R. designed research; S.K.C., A.Y., H.K., R.S., F.C., and M.K. performed research; S.K.C., A.Y., R.S., F.C., L.M., S.S., and K.R. analyzed data; S.K.C., A.Y., and K.R. wrote the paper.

This research was supported by Israel Science Foundation (ISF) Grants ISF 946/17 and ISF 258/20 (to K.R.).

Acknowledgments: We thank all current members of the Rosenblum labs for their help and support, to the veterinary team headed by Barak Carmi and Corina Dollingher, and technical team headed by Yair Bellehsen. Graphical illustrations were created using BioRender.com.

*S.K.C. and A.Y. contributed equally to this work.

Correspondence should be addressed to Kobi Rosenblum at kobir@psy.haifa.ac.il or Adonis Yiannakas at adonis.yiannakas@gmail.com or Sailendrakumar Kolatt Chandran at sailendrakumarkc@gmail.com.

https://doi.org/10.1523/ENEURO.0302-22.2022

Copyright © 2023 Kolatt Chandran et al.

This is an open-access article distributed under the terms of the Creative Commons Attribution 4.0 International license, which permits unrestricted use, distribution and reproduction in any medium provided that the original work is properly attributed.

memory necessitates the that coupling of intrinsic and synaptic plasticity (Turrigiano, 2011; Greenhill et al., 2015; C. H. Wu et al., 2021).

The IC is an integration hub tuned for the encoding of both exteroceptive as interoceptive information (Gogolla et al., 2014; Haley and Maffei, 2018; Livneh et al., 2020; Koren et al., 2021). By virtue of its extensive network of connectivity, this elongated cortical structure has been shown to integrate sensory, emotional, motivational, and cognitive brain centers through distinct mechanisms. For example, deletions of either *Fos* or *Stk11* in BLA-aIC neurons, alter intrinsic properties at the aIC, and impair CTA acquisition (Levitan et al., 2020). Furthermore, approach behaviors in social decision-making are modulated by subjective and sex-specific affective states that regulate cell-type-specific changes in intrinsic properties at IC projections to the nucleus accumbens (Rogers-Carter et al., 2018, 2019; Rieger et al., 2022). The posterior IC (pIC) integrates visceral-sensory signals of current physiological states with hypothalamus-gated amygdala anticipatory inputs relating to food or water ingestion, to predict future physiological states (Livneh et al., 2017, 2020). Conversely, aversive visceral stimuli such as LiCl, activate CaMKII neurons projecting to the lateral hypothalamus in right-, but not the left IC, whose optogenetic activation or inhibition can bidirectionally regulate food consumption (Y. Wu et al., 2020). We have previously shown that the aIC-BLA projection is necessary and sufficient for CTA acquisition and retrieval (Lavi et al., 2018; Kayyal et al., 2019), while CTA Retrieval requires activation of the projection concomitant with parvalbumin (PV) interneurons (Yiannakas et al., 2021). Moreover, artificial activation of aIC-BLA projecting neurons is sufficient to induce CTA for appetitive taste (Kayyal et al., 2019). Here, using retrograde viral tracing, behavioral analysis, and whole-cell patch-clamp slice electrophysiology, we assessed two hypotheses: (1) that the intrinsic properties of the aIC-BLA projection change as a function of certainty of taste valence prediction, but not percept; and (2) that predictive valence-specific changes in intrinsic properties would be reflected through excitability, being low when taste outcome is highly predictive (i.e., following CTA Retrieval or unreinforced familiarization), and high when taste valence is uncertain (i.e., following novelty or extinction). Our data demonstrate for the first time that the intrinsic properties of LIV–VI aIC-BLA neurons are differentially regulated by innate and learned drives, reflecting the confidence of currently perceived taste valence.

Materials and Methods

Animals

Animals used were 8- to 12-week-old C57BL/6j [wild type (WT)] adult male mice. Mice were kept in the local animal resource unit at the University of Haifa on a 12/12 h light/dark cycle. Water and chow pellets were available *ad libitum*, while ambient temperature was tightly regulated. All procedures conducted were approved by the University of Haifa Animal Care and Use Committee (Ethics License 554/18), as prescribed by the Israeli National Law for the Protection of Animals–Experiments with Animals (1994).

Animal surgery and viral injections

Following surgery and stereotactic injection of viral vectors, behavioral paradigms were performed, as previously described (Yiannakas et al., 2021). Briefly, mice were treated with norocarp (0.5 mg/kg), before being anesthetized (M3000 NBT Israel/Scivena Scientific) and transferred to a Model 963 Kopf stereotactic device. Upon confirming the lack of pain responses, the skull was surgically exposed and drilled to bilaterally inject 0.25 μl of ssAAV_retro2-hSyn1-chi-mCherry-WPRE-SV40p(A) (physical titer 8.7 $\times$ 10E12 vg/ml), at the BLA (AP $-$1.58; ML $\pm$3.375; DV $-$4.80). Viral delivery was performed using a Hamilton micro-syringe (0.1 μl/min), while the sculp was cleaned and closed using Vetbond. Animals were then administered with 0.5 mg/kg norocarp and 0.5 mg/kg of Baytril (enrofloxacin), and then transferred to a clean and heat-adjusted enclosure for 2 h. Upon inspection, mice were returned to fresh cages along with similarly treated cage-mates. Weight-adjusted doses of the Norocarp and Baytril were administered for an additional 3 d. All AAV constructs used in this study were obtained from the Viral Vector Facility of the University of Zurich (http://www.vvf.uzh.ch/).

Electrophysiological studies of the influence of innate taste identity, novelty, and valence on aIC-BLA excitability

WT mice treated with viral constructs labeling aIC-BLA projecting neurons were used for electrophysiological studies. Upon recovery, mice were randomly assigned into treatment groups (Fig. 1). Following 24 h of water deprivation, animals were water restricted for 3 d, receiving water in pipettes *ad libitum* for 20 min/d (Kayyal et al., 2019; Yiannakas et al., 2021). This regime has been extensively used by our lab as it allows rodents to reliably learn to drink from water pipettes with minimal weight loss. Mean total drinking was recorded on the third day of water restriction. Novel taste consumption groups were presented with 1.0 ml of either 0.5% saccharin (*Saccharin 1x*), or Quinine 0.014% (*Quinine 1x*). One hour following the final taste presentation, animals were subjected to patch-clamp electrophysiology (Kayyal et al., 2021; Yiannakas et al., 2021). The *Water* group underwent the same behavioral procedure without novel taste presentations were killed for electrophysiological investigations 1 h following water presentation. To dissociate between taste identity and familiarity-related changes in electrophysiological properties, a cohort of mice treated to label the aIC-BLA projection were similarly water deprived following familiarization with saccharin (*Saccharin 5x*). Following the initial water restriction, *Saccharin 5x* animals were allowed access to 0.5% saccharin, in 20-min sessions for 4 d. On the fifth day, mice were provided with 1.0 ml of the tastant, 1 h before killing for electrophysiological recordings. Additionally, WT animals injected with the same viral vector, were allowed a month to recover, following which they were killed for electrophysiological investigations without any behavioral manipulation (*Cage Controls*).

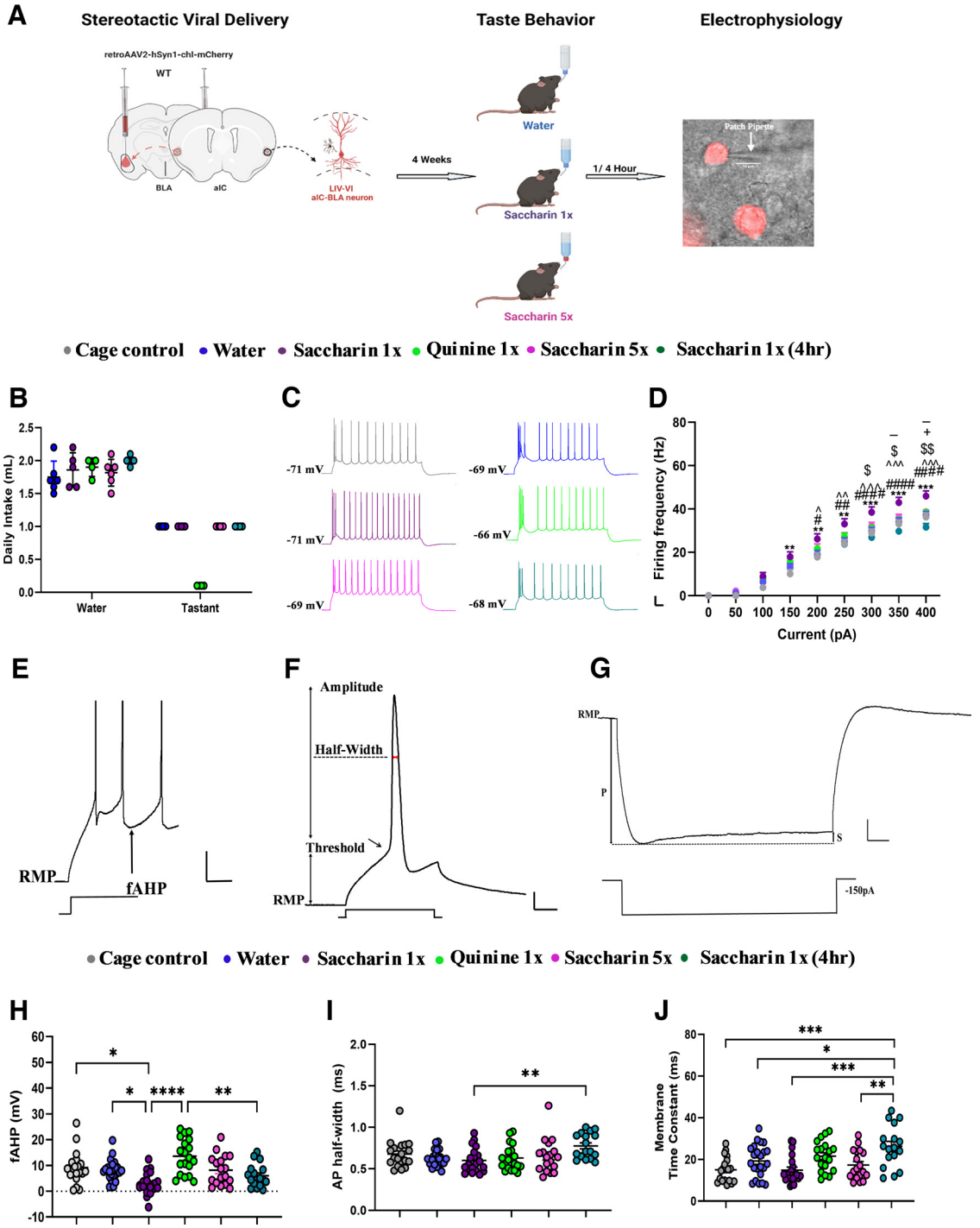

Figure 1. Retrieval of appetitive and novel taste increases excitability in LIV–VI aIC-BLA projection neurons. ***A***, Diagrammatic representation of experimental procedures. Following surgery and stereotaxic delivery of ssAAV_retro2-hSyn1-chi-mCherry-WPRE-SV40p(A) into the BLA, mice were allowed four weeks of recovery. Animals were subsequently assigned to treatment groups and trained to drink from pipettes (see Materials and Methods). We compared the intrinsic properties of LIV–VI aIC-BLA neurons among the Water ($n = 6$ animals, 23 cells), Saccharin 1x ($n = 5$ animals, 20 cells), Saccharin 1x (4 h) ($n = 4$ animals, 17 cells), Saccharin 5x ($n = 6$ animals, 18 cells), and Quinine 1x groups ($n = 4$ animals, 19 cells), as well as a Cage Control group ($n = 4$ animals, 19 cells) that underwent surgery and stereotaxic delivery of ssAAV_retro2-hSyn1-chi-mCherry-WPRE-SV40p(A) at the BLA without water restriction. ***B***, Graph showing the water consumption before treatment (mean ± SD). There was no significant difference between water intakes between the groups before the treatment. One-way ANOVA, $p = 0.9766$. ***C***, Representative traces of LIV–VI aIC-BLA projecting neurons from the six treatment groups. Scale bars: 20 mV vertical and 50 ms horizontal from 300-pA step. ***D***, The dependence of firing rate on current step magnitude in LIV–VI aIC-BLA neurons was significantly different among the treatment groups. Excitability in the Saccharin 1x was increased compared with all other groups. Two-way repeated measures ANOVA,

continued

Current × Treatment: $p < 0.0001$; Cage Control versus Saccharin 1x: **$p < 0.01$, ***$p < 0.001$; Saccharin 1x versus Saccharin 1x (4 h): #$p < 0.05$, ##$p < 0.01$, ####$p < 0.0001$; Water versus Saccharin 1x: ^$p < 0.05$, ^^$p < 0.01$, ^^^$p < 0.001$; Saccharin 1x versus Quinine 1x: \$$p < 0.05$, \$\$$p < 0.01$; Saccharin 1x versus Saccharin 5x: -$p < 0.05$; Saccharin 1x (4 h) versus Saccharin 5x: +$p < 0.05$. ***E***, Representative of all fAHP measurements in response to 500-ms step current injections. Scale bars: 20 mV vertical and 50 ms horizontal. ***F***, Representative of all action potential properties were taken. Scale bars: 20 mV vertical and 5 ms horizontal. ***G***, Measurements for all input resistance, sag ratio, and membrane time constants were analyzed in response to 1-s, −150-pA step current injection. P, peak voltage; S, steady state voltage. Scale bars: 5 mV vertical and 100 ms horizontal. ***H***, Significant differences were observed among the treatment groups in terms of fAHP. Cage Control (9.191 ± 1.449 mV), Water (8.150 ± 0.8288 mV), Saccharin 1x (3.016 ± 0.9423 mV), Quinine 1x (13.58 ± 1.562 mV), Saccharin 5x (8.158 ± 1.356 mV), Saccharin 1x (4 h) (5.989 ± 1.074 mV), one-way ANOVA, $p < 0.0001$. ***I***, Action potential half-width in the Saccharin 1x group (0.6005 ± 0.03260 ms) was significantly decreased compared with Saccharin 1x (4 h) (0.7765 ± 0.03641 ms), one-way ANOVA, $p = 0.0065$. ***J***, The membrane time constant was significantly different between the Cage Control (15.03 ± 1.376 ms) and Saccharin 1x (4 h) (26.21 ± 2.421 ms), Water (19.24 ± 1.620 ms) and Saccharin 1x (4 h) (26.21 ± 2.421 ms), Saccharin 1x (14.82 ± 1.485 ms) and Saccharin 1x (4 h) (26.21 ± 2.421 ms), and Saccharin 5x (17.30 ± 1.660 ms) and Saccharin 1x (4 h) (26.21 ± 2.421 ms) groups. One-way ANOVA, $p < 0.0001$. For panels ***D***, ***H–J***: *$p < 0.05$, **$p < 0.01$, ***$p < 0.001$, ****$p < 0.0001$. All data are shown as mean ± SEM. Histologic verification of viral delivery at the IC and BLA, as well as locations of whole-cell patch-clamp recording electrode (see Extended Data Fig. 1-1). Individual IC neurons were classified as burst-spiking and regular-spiking by *post hoc* analysis of responses to rheobase current injections (see Extended Data Fig. 1-2). The intrinsic properties of burst spiking LIV–VI aIC-BLA projecting neurons are differentially modulated by taste valence in the context of novelty (see Extended Data Fig. 1-3).

Electrophysiological studies of the influence of learned aversive taste memory retrieval on aIC-BLA excitability

WT mice were treated with viral constructs labeling aIC-BLA projecting neurons to assess the electrophysiological properties of the projection during aversive or appetitive taste memory retrieval. Upon recovery, mice in CTA Retrieval group were trained in CTA for saccharin (LiCl 0.14 M, 1.5% body weight), while the appetitive saccharin retrieval group (*Saccharin 2x*) received a matching body weight adjusted injection of saline (Yiannakas et al., 2021). Three days following conditioning, both groups underwent a memory retrieval task, receiving 1.0 ml of the conditioned tastant 1 h before killing (Figs. 2, 3 and 4). Brain tissue was extracted and prepared for electrophysiological recording, as above.

Electrophysiological studies of the influence of learned aversive taste memory extinction and reinstatement on aIC-BLA excitability

Electrophysiological studies of CTA extinction and reinstatement were conducted in a cohort of WT male mice (Yiannakas et al., 2021). Following surgery, recovery and water restriction, animals were randomly assigned to the extinction and reinstatement groups (Figs. 3, 4). The aversion index for the extinction and reinstatement groups were calculated by the formula:

$$\text{Aversion index} = \left[\frac{\textit{Volume of water}}{\textit{volume of (water + tastant)}}\right] * 100.$$

Adult male mice used to study extinction and reinstatement were trained in CTA for saccharin following extinction, the reinstatement group received an identical intraperitoneal dose to the original unconditioned stimulus (LiCl 0.14 M, 1.5% body weight), 24 h before retrieval. Conversely, the extinction group received a similarly weight-adjusted dose of saline. During the final retrieval session, both groups of mice were allowed access to 1.0 ml of the CS, 1 h before killing under deep anesthesia and slice preparation for electrophysiology.

Electrophysiology tissue preparation

The slice electrophysiology and recording parameters were used as described previously (Kayyal et al., 2021; Yiannakas et al., 2021). Briefly, mice were deeply anesthetized using isoflurane, while brains were extracted following decapitation. Three-hundred um thick coronal brain slices were obtained with a Campden-1000 Vibratome. Slices were cut in ice-cold sucrose-based cutting solution containing the following (in mM): 110 sucrose, 60 NaCl, 3 KCl, 1.25 NaH_2PO_4, 28 $NaHCO_3$, 0.5 $CaCl_2$, 7 $MgCl_2$, 5 D-glucose, and 0.6 ascorbate. The slices were allowed to recover for 30 min at 37°C in artificial CSF (ACSF) containing the following (in mM): 125 NaCl, 2.5 KCl, 1.25 NaH_2PO_4, 25 $NaHCO_3$, 25 D-glucose, 2 $CaCl_2$, and 1 $MgCl_2$. Slices were then kept for an additional 30 min in ACSF at room temperature until electrophysiological recording. The solutions were constantly gassed with carbogen (95% O_2, 5% CO_2).

Intracellular whole-cell recording

After the recovery period, slices were placed in the recording chamber and maintained at 32–34°C with continuous perfusion of carbogenated ACSF (2 ml/min). Brain slices containing the anterior insular cortices were illuminated with infrared light and pyramidal cells were visualized under a differential interference contrast microscope with 10× or 40× water-immersion objectives mounted on a fixed-stage microscope (BX51-WI; Olympus). The image was displayed on a video monitor using a charge-coupled device (CCD) camera (QImaging). Insula to BLA projection cells infected with AAV were identified by visualizing $mCherry^+$ cells. Recordings were amplified by Multiclamp Axopatch 200B amplifiers and digitized with Digidata 1440 (Molecular Devices). The recording electrode was pulled from a borosilicate glass pipette (3–5 M) using an electrode puller (P-1000; Sutter Instruments) and filled with a K-gluconate-based internal solution containing the following (in mM): 130 K-gluconate, 5 KCl, 10 HEPES, 2.5 $MgCl_2$, 0.6 EGTA, 4 Mg-ATP, 0.4 Na3GTP, and 10 phosphocreatine (Na salt). The osmolarity was 290 mOsm, and pH was 7.3. The recording glass pipettes were

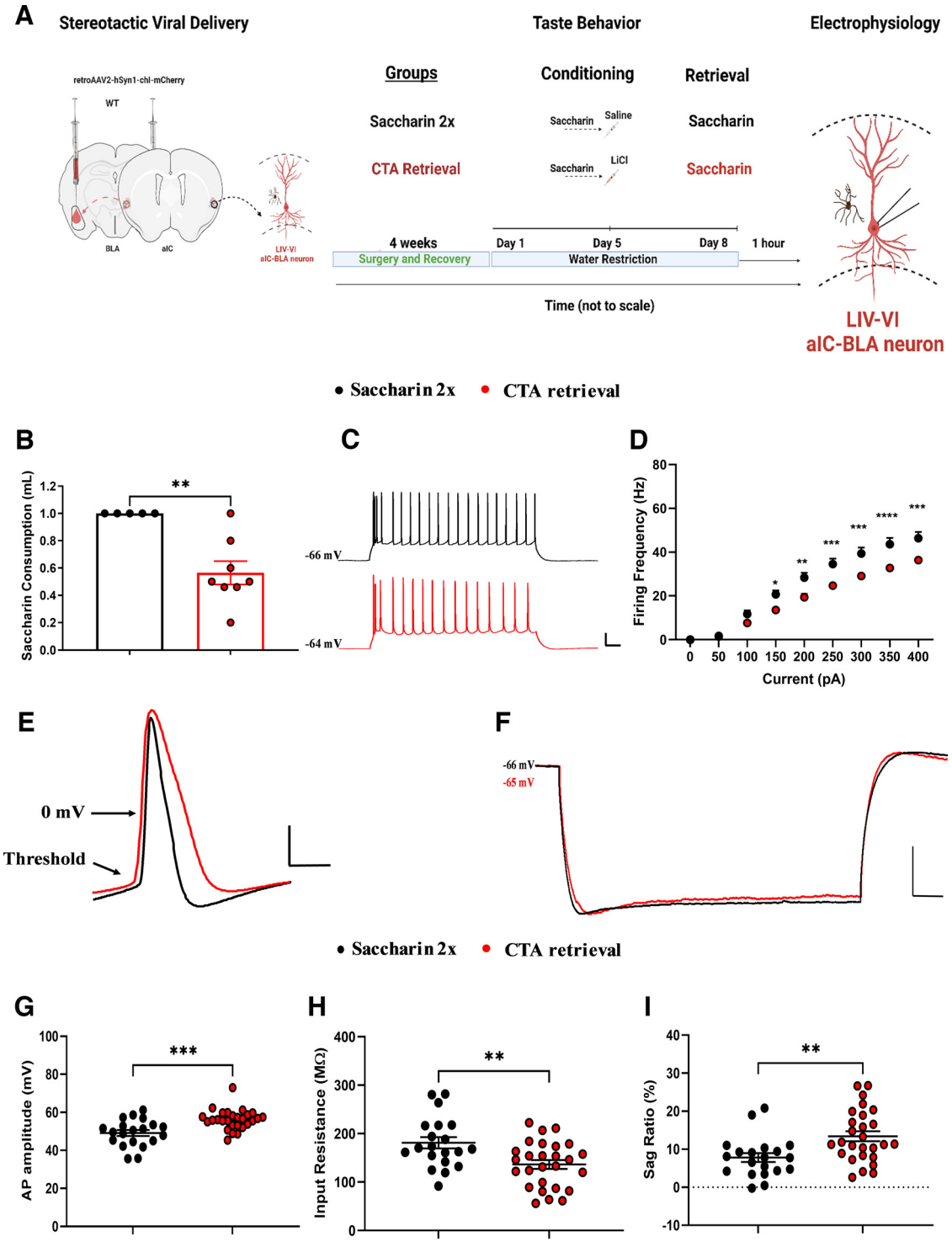

Figure 2. Learned aversive taste memory retrieval decreases the excitability of LIV–VI aIC-BLA projecting neurons. ***A***, Experimental design of behavioral procedures conducted to compare the intrinsic properties of LIV–VI aIC-BLA neurons following learned aversive taste memory retrieval (CTA Retrieval, $n = 8$ animals, 27 cells), appetitive retrieval for the same tastant (Saccharin 2x, $n = 5$ animals, 20 cells). ***B***, Mice showed a significantly reduced saccharin consumption following learned aversive memory retrieval ($n = 8$) compared with appetitive retrieval mice ($n = 5$) group. $p = 0.0085$, Mann–Whitney test. ***C***, Representative traces of LIV–VI aIC-BLA projecting neurons from the two treatment groups. Scale bars: 20 mV vertical and 50 ms horizontal from 300-pA step. ***D***, The excitability of LIV–VI aIC-BLA in the Saccharin 2x group was significantly enhanced compared with CTA Retrieval. Two-way repeated measures ANOVA, Current × Treatment: $p < 0.0001$. ***E***, Representative traces showing action potential measurements for both groups. Scale bar: 20 mV vertical and 2 ms horizontal. ***F***, Representative traces showing the input resistance and sag ratio measurements. Scale bar: 10 mV vertical and 100 ms horizontal. ***G***, Action potential amplitude in the CTA Retrieval (56.21 ± 0.9978 mV)

continued

group was increased compared with Saccharin 2x (49.14 ± 1.568 mV), $p = 0.0005$, Mann–Whitney test. ***H***, Input resistance in the CTA Retrieval group (136.4 ± 9.064 MΩ) was significantly decreased compared with Saccharin 2x (181.1 ± 11.7 MΩ). $p = 0.0036$, Unpaired *t* test. ***I***, SAG ratio following CTA Retrieval (13.41 ± 1.31) was significantly enhanced compared with Saccharin 2x (7.815 ± 1.176). $p = 0.0037$, Unpaired *t* test. Data are shown as mean ± SEM $^{*}p < 0.05$, $^{**}p < 0.01$, $^{***}p < 0.001$, $^{****}p < 0.0001$. Learned aversive taste memory retrieval decreases the excitability of burst spiking LIV–VI aIC-BLA neurons (see Extended Data Fig. 2-1).

patched onto the soma region of mCherry^{+} pyramidal neurons and neighboring non fluorescent pyramidal neurons.

The recordings were made from the soma of insula pyramidal cells, particularly from layer 2/3 and layer 5/6. Liquid junction potential (10 mV) was not corrected online. All current clamp recordings were low pass filtered at 10 kHz and sampled at 50 kHz. Pipette capacitance and series resistance were compensated and only cells with series resistance smaller than 20 MΩ were included in the dataset. Data quantification was done with Clampfit (Molecular Devices) and subsequently analyzed using GraphPad Prism. The method for measuring active intrinsic properties was based on a modified version of previous protocols (Kaphzan et al., 2013; Chakraborty et al., 2017; Sharma et al., 2018).

Recording parameters

Resting membrane potential (RMP) was measured 10 s after the beginning of whole-cell recording (rupture of the membrane under the recording pipette). The dependence of firing rate on the injected current was obtained by injection of current steps (of 500-ms duration from 0 to 400 pA in 50-pA increments). Input resistance was calculated from the voltage response to a hyperpolarizing current pulse (−150 pA). SAG ratio was calculated from voltage response −150 pA. The SAG ratio during the hyperpolarizing steps was calculated as $[(1 - \Delta V_{SS}/\Delta V_{max}) \times 100\%]$ as previously reported by (Song et al., 2015). The membrane time constant was determined using a single exponential fit in the first 100 ms of the raising phase of cell response to a 1 s, −150-pA hyperpolarization step.

For measurements of a single action potential (AP), after initial assessment of the current required to induce an AP at 15 ms from the start of the current injection with large steps (50 pA), a series of brief depolarizing currents were injected for 10 ms in steps of 10-pA increments. The first AP that appeared on the 5-ms time point was analyzed. A curve of dV/dt was created for that trace and the 30 V/s point in the rising slope of the AP was considered as threshold (Chakraborty et al., 2017). AP amplitude was measured from the equipotential point of the threshold to the spike peak, whereas AP duration was measured at the point of half-amplitude of the spike. The medium after-hyperpolarization (mAHP) was measured using prolonged (3 s), high-amplitude (3 nA) somatic current injections to initiate time-locked AP trains of 50 Hz frequency and duration (10 –50 Hz, 1 or 3 s) in pyramidal cells. These AP trains generated prolonged (20 s) AHPs, the amplitudes and integrals of which increased with the number of APs in the spike train. AHP was measured from the equipotential point of the threshold to the anti-peak of the same spike (Gulledge et al., 2013). Fast (fAHP), and slow AHP (sAHP) measurements were identified as previously described (Andrade et al., 2012; Song and Moyer, 2018). Series resistance, Rin, and membrane capacitance were monitored during the entire experiment. Changes of at least 30% in these parameters were criteria for exclusion of data.

Classification of burst and regular spiking neurons

At the end of recordings, neurons were classified as either burst (BS) or regular spiking (RS) as reported previously (Kim et al., 2015; Song et al., 2015). Briefly, neurons that fired two or more action potentials (doublets or triplets) potential toward a depolarizing current step above the spike threshold current were defined as burst spiking (BS). Regular spiking (RS) neurons on the other hand, were defined as neurons that fired single action potential in response to a depolarizing current step above spike threshold (Extended Data Fig. 1-2*A*).

Statistical analysis of individual intrinsic properties across treatments

Group size was based on previously published results using similar methods (Gould et al., 2021; Kayyal et al., 2021), as well as through conducting power analysis calculations, to obtain power ≥ 0.8 with $\alpha = 0.05$ (https://www.stat.ubc.ca/~rollin/stats/ssize/n2.html). Individual intrinsic properties of aIC-BLA projecting neurons in the respective treatment groups (Figs. 1-4) were analyzed using appropriate statistical tests (one-way or two-way ANOVA, GraphPad Prism), as defined in the Table 5, statistics table. Two-way repeated measurements of ANOVA (RM-ANOVA) followed by Šídák's (for two groups) or Tukey's (for more than two groups) *post hoc* multiple comparison test was performed for firing properties. The intrinsic properties were determined with two-tailed unpaired *t* tests, and one-way ANOVA followed by Tukey's or Dunn's multiple comparisons test were used. For all tests, $^{*}p < 0.05$ was considered significant. D'Agostino and Pearson test used for the identifying the normal distribution of the data. Multiple comparisons were corrected *post hoc* with Tukey's for one-way/two-way ANOVA and Dunn's for Kruskal–Wallis test.

Following spike-sorting, the ratio of BS:RS aIC-BLA projecting neurons in the sampled population was compared across our treatments (Mann–Whitney test, GraphPad Prism). Similarly, individual intrinsic properties in BS and RS aIC-BLA projecting neurons were analyzed following spike-sorting (one-way or two-way ANOVA, GraphPad Prism). All data reported as mean ± SEM.

Immunohistochemistry

From each electrophysiological recording, three 300-μm-thick mouse brain slices were obtained starting from

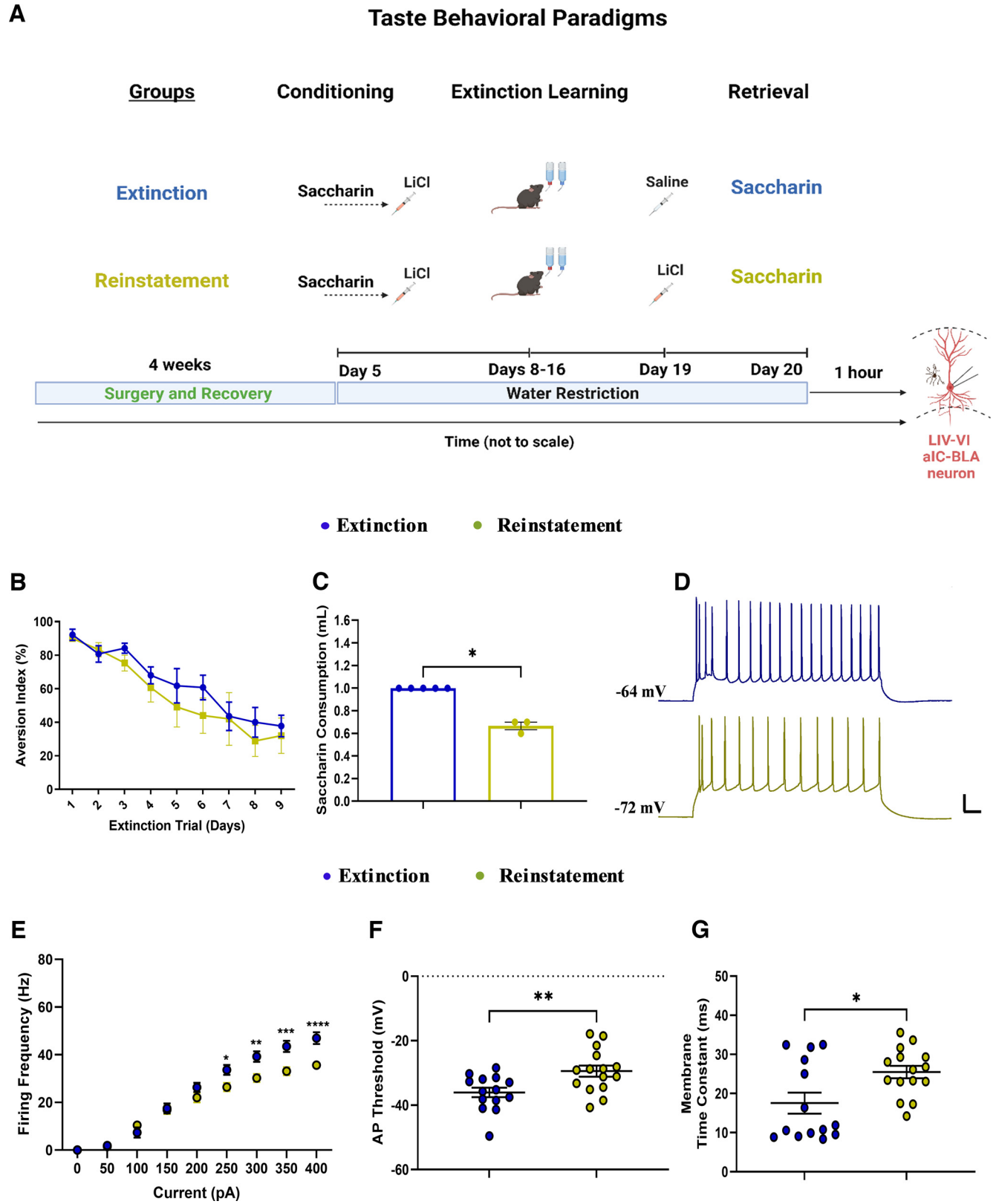

Figure 3. Extinction of CTA enhances, whereas reinstatement decreases, the excitability of LIV–VI aIC-BLA projecting neurons. ***A***, Experimental design of behavioral procedures conducted to compare the intrinsic properties of LIV–VI aIC-BLA neurons following CTA Extinction ($n = 5$, animals, 14 cells) and Reinstatement ($n = 3$ animals, 15 cells). ***B***, The graph showing the reduced aversion following the successful extinction in both treatment groups. ***C***, Data showing the saccharin consumption on the test day following successful extinction and Reinstatement of CTA. CTA reinstated mice showed significantly reduced saccharin consumption

continued

compared with extinguished mice. $p = 0.0179$, Mann–Whitney test. ***D***, Representative traces of LIV–VI aIC-BLA projection neurons firing from the two treatment groups. Scale bars: 20 mV and 50 ms horizontal from 300-pA step. ***E***, Excitability in LIV–VI aIC-BLA neurons was significantly different among the treatment groups. Two-way repeated measures ANOVA, Current × Treatment: $p < 0.0001$. ***F***, Action potential threshold in the Reinstatement group (-29.43 ± 1.731 mV) was enhanced compared with Extinction (-36.06 ± 1.481 mV). $p = 0.0076$, Unpaired *t* test. ***G***, The membrane time constant following Reinstatement (25.48 ± 1.58 ms) was significantly enhanced compared with Extinction (17.55 ± 2.684 ms, $p = 0.047$). $p = 0.0153$, Unpaired *t* test. For panels ***D–F***: $^{*}p < 0.05$, $^{**}p < 0.01$, $^{***}p < 0.001$, $^{****}p < 0.0001$. All data are shown as mean ± SEM. Extinction of CTA enhances the excitability of burst spiking LIV–VI aIC-BLA projecting neurons compared with CTA reinstatement (see Extended Data Fig. 3-1).

bregma coordinates 1.78, 1.54, and 1.18, respectively. Slices were washed with PBS and fixed using 4% paraformaldehyde in PBS at 4°C for 24 h. Slices were then transferred to 30% sucrose/PBS solution for 48 h and mounted on glass slides using Vectashield mounting medium with DAPI (H-1200). Slides were then visualized using a vertical light microscope at 10× and 20× magnification (Olympus CellSens Dimension). Images were processed using Image-Pro Plus V-7 (Media Cybernetics). The localization of labeled mCherry+ neurons in the agranular aIC, where recordings were obtained from, was quantified manually across three bregma-matched slices, for each animal. Quantification was done using randomly assigned IDs for individual animals, regardless of treatment. Representative images were additionally processed using the Olympus CellSens 2-D deconvolution function.

Principal component analysis (PCA) of the profile of intrinsic properties across treatment groups

Principal component analysis (PCA) of the standardized intrinsic properties of the LIV–VI aIC-BLA (Fig. 5; Extended Data Fig. 5-1) was performed using the correlation matrix on GraphPad Prism9, MATLAB R2020b, and IBM SPSS Statistics 27. The covariance matrix was used for each PCA was performed in six behavioral groups, the low memory prediction (Saccharin 1x, $n = 20$; Saccharin 2x, $n = 20$, and Extinction, $n = 14$), and the high memory prediction (Saccharin 5x, $n = 18$; CTA Retrieval, $n = 27$, and Reinstatement, $n = 15$), RS versus BS neurons. A total of 114 neurons (BS vs RS) across all intrinsic properties and excitability changes (50–400 pA; Extended Data Fig. 5-1*A*), and later all intrinsic properties with only 350 pA (highest excitability differences between treatment groups; Extended Data Fig. 5-1*B*). PCA was conducted on 63 burst spiking neurons using 12 variables: 350 (pA), RMP (mV), mAHP (mV), sAHP (mV), fAHP (mV), IR (MΩ), SAG Ratio, Time constants (ms), AP amplitude (mV), AP Halfwidth (ms), AP threshold (mV), Rheobase (pA; Fig. 5*A*,*B*). The adequacy of the sample was evaluated using the Bartlett's test and the Kaiser–Meyer–Olkin (KMO) measure was applied. The degrees of freedom (df) were calculated using the following formula:

$$df = \sharp variables - 1.$$

The number of principal components was chosen according to the percentage of variance explained (>75%). The parallel analysis evaluated the optimal number of components and selected three PCs, explaining 62.47% of the variance. Oblique factor rotation (par) of the first three PCA components, using a standard "rotatefactors" routine from MATLAB Statistics Toolbox. This approach maximizes the varimax criterion using an orthogonal rotation. To optimize variance, oblique factor rotation (paramax) was used, and the threshold chosen to define a variable as a significant contributor was a variance ≥0.7 given the small sample size. The correlation matrix was adequate as the null hypothesis of all zero correlation was rejected ($\chi_{66}^2 = 387.444$, $p < 0.001$), and KMO exceeded 0.5 (KMO = 0.580).

To calculate the proportion of the variance of each variable that the principal components can explain, communalities were calculated and ranged from 0.426 to 0.897 (Extended Data Fig. 5-1*A–C*). The communalities scores were calculated using the following formula: $= \frac{\sum_{i=1}^{m} \lambda}{\sharp variables * \lambda}$; where *m* is the number of selected PCs. The threshold chosen was Comm ≥ 60%.

Because of the imbalance in sample sizes between groups, the PCA space is biased in favor of the group with bigger sample size. The BS neurons in the six behavioral groups previously mentioned were resampled to ensure that sample sizes were balanced across groups datasets (Fig. 5*A*,*B*). Particularly, we reduced the number of Saccharin 1x and 2x observations by using random sampling ("randn" function in MATLAB); for Saccharin 1x, we chose 10 of the 17 total elements, and for Saccharin 2x, we selected 10 of the 13 total elements.

K-means clustering

Unbiased clustering analysis based on the K-means algorithm was conducted to search for an optimal division of samples into a predetermined number of clusters within an unlabeled multidimensional data set (MacQueen, 1967). In the present study we chose K-means clustering methods to cluster the similar groups into a high and low predictive valance outcome following the memory, based on their intrinsic properties. As a popular method for a cluster analysis, K-means clustering aims to partition n observations into k–clusters in which each observation belongs to the cluster with the nearest mean, serving as a prototype of a cluster. In this classification a set of clustering results with different number of clusters can be calculated by setting a different k. The final step is to determine the optimal dimension which gives the best classification. To assess the distribution of bursting neurons in multidimensional space, we performed a k-means cluster analysis in MATLAB for the principal components (k = 2 clusters, maximum

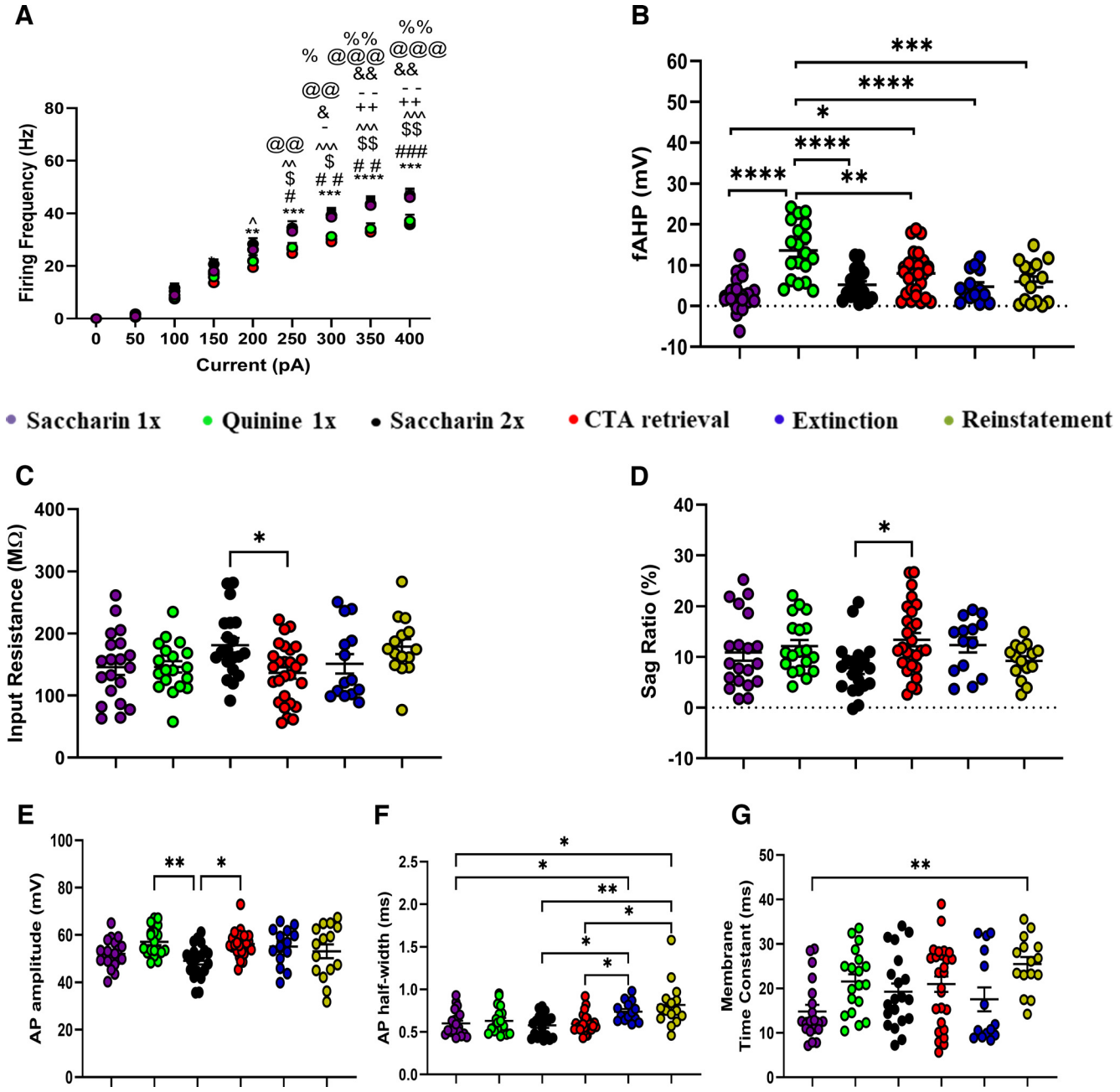

Figure 4. Innately aversive taste is correlated with high fAHP, and prolonged conflicting experiences is correlated with an increased AP half-width in LIV–VI aIC-BLA projecting neurons. We compared the intrinsic properties of LIV–VI aIC-BLA neurons among the Saccharin 1x ($n = 5$ animals, 20 cells), Quinine 1x ($n = 4$ animals, 19 cells), Saccharin 2x ($n = 5$ animals, 20 cells), CTA Retrieval ($n = 8$, 27 cells), Extinction ($n = 5$ animals, 14 cells), and Reinstatement ($n = 3$ animals, 15 cells) groups. ***A***, Groups associated with positive taste valence (Saccharin 1x, Saccharin 2x, Extinction), exhibited significantly increased excitability compared with innate or learned negative taste valence groups (Quinine 1x, CTA Retrieval, and Reinstatement). Two-way repeated measures ANOVA, Current × Treatment: $p < 0.0001$; Saccharin 2x versus CTA Retrieval: *p; Saccharin 2x versus Reinstatement: #p: Saccharin 2x versus Quinine 1x: p$; Saccharin 1x versus CTA Retrieval: p^; Saccharin 1x versus Quinine 1x: p%; Saccharin 1x versus reinstatement: p+; Extinction versus CTA Retrieval: p@; Extinction versus Reinstatement: p&; Extinction versus Quinine 1x: p-. ***B***, fAHP was significantly enhanced in response to Quinine 1x (13.56 ± 1.562 mV) compared with all other groups. Significant differences were also observed between Saccharin 1x (3.016 ± 0.9423 mV), Saccharin 2x (5.223 ± 0.8217 mV), and CTA Retrieval (7.97 ± 1.018 mV, $p = 0.0036$). Extinction (4.731 ± 1.021 mV) and Reinstatement (5.932 ± 1.292 mV). One-way ANOVA, $p < 0.0001$. ***C***, Input resistance was significantly different between Saccharin 2x (181.1 ± 11.7 MΩ) and CTA Retrieval (136.4 ± 9.064 MΩ), $p = 0.0352$. Conversely, input resistance in Saccharin 1x (145.8 ± 12.56), Quinine 1x (146 ± 9.094), Extinction (151.1 ± 15.63), and Reinstatement groups was similar. One-way ANOVA, $p = 0.0213$. ***D***, SAG ratio was significantly different between Saccharin 2x (7.815 ± 1.176) and CTA Retrieval (13.41 ± 1.31), $p = 0.0209$. Conversely, SAG ratio in Saccharin 1x (10.89 ± 1.621), Quinine 1x (12.13 ± 1.23), Extinction (12.37 ± 1.471), and Reinstatement (9.245 ± 0.884) groups was similar one-way ANOVA, $p = 0.0286$. ***E***, Action potential amplitude

continued
in the Quinine 1x group (57.11 ± 1.376 mV), and CTA Retrieval (56.21 ± 0.9978 mV), was significantly increased compared with Saccharin 2x (49.14 ± 1.568 mV, p = 0.0175 and 0.0229, respectively). Conversely, action potential attitude in the Saccharin 1x (52.03 ± 1.308 mV), Extinction (55.09 ± 2.122 mV), and Reinstatement (53.1 ± 2.906 mV) groups was similar. One-way ANOVA, $p = 0.0061$. ***F***, Action potential half-width following Extinction (0.7386 ± 0.03145 ms) and Reinstatement (0.8187 ± 0.06929 ms) was elevated compared with Saccharin 1x (0.6005 ± 0.03260 ms), Saccharin 2x (0.5780 ± 0.02994 ms) as well as CTA Retrieval (0.5959 ± 0.02080 ms, but no with Quinine 1x (0.6300 ± 0.03555 ms). One-way ANOVA, $p = 0.0002$. ***G***, The membrane time constant in the Saccharin 1x (14.82 ± 1.485 ms) group was significantly decreased compared with Reinstatement (25.48 ± 1.58 ms, p = 0.0043) groups was. Differences between CTA Retrieval (20.96 ± 1.724 ms, $p = 0.0189$), Quinine 1x (21.55 ± 1.638 ms), Saccharin 2x (19.28 ± 1.837 ms), and Extinction (17.55 ± 2.684 ms) groups failed to reach significance. One-way ANOVA, $p = 0.0047$.

iterations was 100 with random starting locations, squared Euclidean distance metric used), which explained 62.47% of the variance in intrinsic properties (Fig. 5; Extended Data Figs. 5-1, 5-2).

Data availability

All data generated or analyzed during this study are included in the manuscript and supporting files. Source data files have been provided for all figures as Extended Data 1.

Results

To prove or refute our hypotheses, we conducted a series of electrophysiological recordings in slice preparation from the mouse aIC, in which we labeled aIC-BLA projecting neurons using retrograde adeno-associated viral tracing – retro AAV (see Materials and Methods). Electrophysiological recordings were obtained from the aIC-BLA projecting neurons in LI–III (Table 1) and LIV–VI (Table 2), following novel appetitive or aversive taste stimuli (Fig. 1), following appetitive or aversive taste memory retrieval (Fig. 2), as well as following extinction and reinstatement (Figs. 3, 4). We focused on deep-lying LIV–VI aIC-BLA projecting neurons (Table 2), as intrinsic properties in superficial LI–III aIC-BLA projecting neurons were unaffected by taste identity, familiarity, or valence (Table 1). We measured action potential (AP) firing frequency in response to incrementally increasing depolarizing current injections, as well as 11 distinct of intrinsic properties (Tables 2-Table 4 and 5, statistics table): resting membrane potential (RMP); slow, medium, and fast after-hyperpolarization (sAHP, mAHP, fAHP); input resistance (IR), SAG ratio; the amplitude, half-width and threshold for APs; the time taken for a change in potential to reach 63% of its final value (membrane time constant, τ), as well as the minimum current necessary for AP generation (Rheobase). Statistical analysis was conducted using repeated measures one-way or two-way ANOVA (see Table 5, statistics table).

When taste is both appetitive and novel, excitability in LIV–VI aIC-BLA projection neurons is increased

To delineate the mechanisms through which novelty is encoded on the LIV/VI aIC-BLA projection, we labeled the projection (see Materials and Methods), and compared the intrinsic properties across neutral, innately aversive, and innately appetitive taste stimuli. Following surgery recovery mice were randomly assigned to the following behavioral groups: Water (Control for procedure, Water; $n = 6$ animals, 23 cells), 0.5% Saccharin for the first (Novel innate appetitive, Saccharin 1x; $n = 5$ animals, 20 cells), or fifth time (Familiar appetitive, Saccharin 5x; $n = 6$ animals, 18 cells), 0.04% Quinine (Novel aversive, Quinine 1x; $n = 4$ animals, 19 cells), or Cage Controls that did not undergo water-restriction (Baseline control, Cage control; $n = 4$ animals, 19 cells). This approach allowed us to examine excitability changes that relate to the innate aversive/appetitive nature and novelty/familiarity associated with tastants, while accounting for the effects of acute drinking, as well as the water restriction regime itself. Guided by evidence regarding the induction of plasticity cascades, the expression of immediate early genes, as well as the timeframes involved in LTP and LTD in IC neurons (Rosenblum et al., 1997; Hanamori et al., 1998; Jones et al., 1999; Escobar and Bermúdez-Rattoni, 2000), the five treatment groups were killed 1 h following taste consumption. Although changes in activity can be observed within seconds to minutes, depending on their novelty, salience, and valence (Barot et al., 2008; Lavi et al., 2018; Y. Wu et al., 2020), sensory experiences can modulate the function of IC neurons for hours (Juárez-Muñoz et al., 2017; Rodríguez-Durán et al., 2017; Haley et al., 2020; Kayyal et al., 2021; Yiannakas et al., 2021). We had previously identified a CaMKII-dependent short-term memory trace at the IC that last for the first 3 h following taste experiences, regardless of their valence (Adaikkan and Rosenblum, 2015). To address whether similar time-dependency of the physiological correlations engaged by the IC during novel taste learning, a sixth group was killed 4 h following novel saccharin exposure [Fig. 1, Saccharin 1x (4 h)].

Daily water intake before the final taste exposure and was not different among the five groups that underwent water restriction (Fig. 1*B*, one-way ANOVA, $p = 0.4424$, $F = 0.9766$, $R^2 = 0.1634$). However, excitability in response to incremental depolarizing currents was significantly different between the six groups (Fig. 1*D*; two-way ANOVA, $p < 0.0001$, $F_{(8,880)} = 1269$). Exposure to saccharin for the first time (i.e., novel appetitive), at the 1-h time point, resulted in enhanced excitability on the aIC-BLA projection compared with all other groups (Fig. 1*D*; see Table 2). Conversely, fAHP (Fig. 1*H*; one-way ANOVA, $p < 0.0001$, $F = 8.380$, $R^2 = 0.2758$) in the Quinine 1x group was increased compared with all other groups, in contrast to Saccharin 1x where it was most decreased (Table 2). In fact, fAHP in the Saccharin groups recorded at 1 h ($p < 0.0001$, z = 5.150) or 4 h ($p = 0.0099$, z = 3.406) following novel taste consumption was decreased compared with innately aversive Quinine 1x (Fig. 1*H*). Although fAHP in the Saccharin 1x group was decreased compared

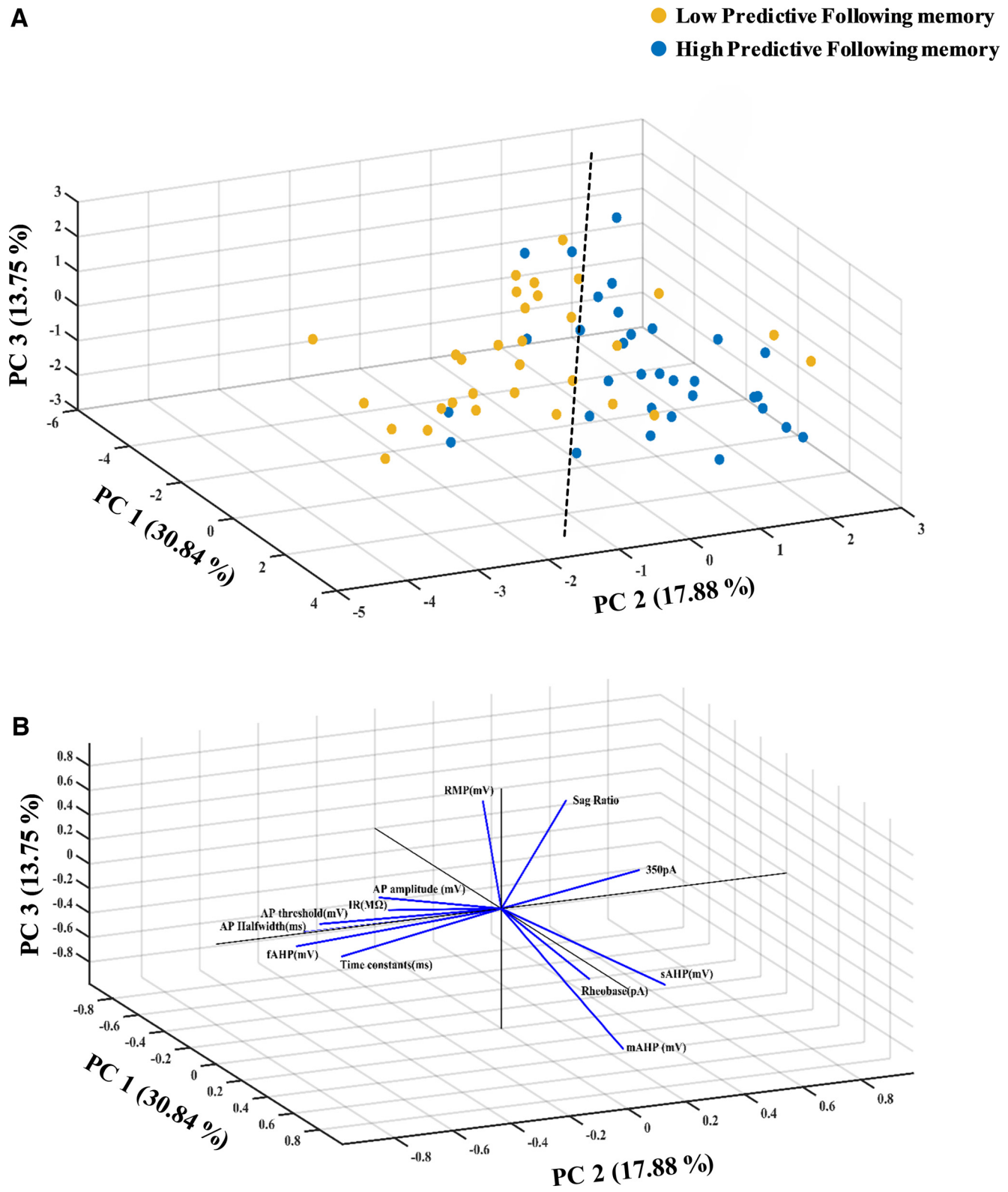

Figure 5. The intrinsic properties of burst spiking LIV–VI aIC-BLA projecting neurons represent taste experience and the probability for further learning. ***A***, Data across all intrinsic properties from BS LIV–VI aIC-BLA neurons of the Saccharin 1x, Saccharin 2x, and Extinction groups were combined and assigned to the Low predictive following memory group (32 BS cells). Conversely, the intrinsic properties of BS LIV–VI aIC-BLA neurons from animals having undergone CTA Retrieval, 5× Saccharin, and Reinstatement were combined and assigned to the High predictive following memory group (31 BS cells). The resultant three-dimensional scatter representation of the two groups

continued

encompassed Excitability at 350 pA; AP amplitude, AP halfwidth, AP threshold; fAHP, mAHP, sAHP; IR, Rheobase, RMP, SAG ratio and τ in BS LIV–VI aIC-BLA neurons. See Extended Data Figure 5-1. ***B***, Three-dimensional representation of the contribution of individual parameters (loadings matrix) to the principal components segregating the two groups of treatments (scores matrix). PCA variable contributions and component loadings of BS and RS LIV–VI aIC-BLA projecting neurons in Extended Data Figure 5-2.

with both the Cage Control ($p = 0.0136$, z = 3.318) and Water ($p = 0.0177$, z = 3.243) groups, this was not the case for the Saccharin 1x (4 h) group ($p > 0.9999$ for both; Table 2). Importantly, fAHP (Fig. 1*H*) was nearly identical in treatment groups where the tastant could be deemed as highly familiar and safe, such as the Cage Control group (that did not undergo water restriction), as well as animals in the Water or Saccharin 5x groups (that had undergone water restriction).

Significant differences in terms of τ (Fig. 1*J*; one-way ANOVA, $p < 0.0001$, $F_{(5,110)} = 6.094$; R^2, 0.2169), were observed between the Cage Control and Saccharin 1x (4 h) groups ($p = 0.0003$, q = 6.326), Water versus Saccharin 1x (4 h) ($p = 0.0488$, q = 4.115), Saccharin 1x and Saccharin 1x (4 h) groups ($p = 0.0002$, q = 6.521), and Saccharin 5x versus Saccharin 1x (4 h), p = (0.0081, q = 4.975, df = 110). On the other hand, significant differences in AP half-width (Fig. 1*I*; Kruskal–Wallis test; $p = 0.0125$, Kruskal–Wallis statistic = 14.54) were only observed between the Saccharin 1x (4 h) compared with Saccharin 1x ($p = 0.0065$, z = 3.519) groups (Table 2).

These results demonstrate that in the context of taste novelty, innately appetitive saccharin drove increases in excitability and decreases in fAHP of LIV–VI aIC-BLA projecting neurons, compared with innately aversive quinine (Fig. 1*D*,*H*). Compared with the Cage Control and Water groups, fAHP on the projection was significantly enhanced by innately aversive quinine and was decreased by innately appetitive novel saccharin (Fig. 1*H*). However, the effect of appetitive taste novelty on firing frequency was time dependent, as it was observed at 1 h, but not 4 h, following novel taste exposure (Fig. 1*D*). Furthermore, following familiarity acquisition for saccharin (Saccharin 5x), excitability was decreased compared with Saccharin 1x, matching the Cage Control, Water, and Quinine 1x groups (Fig. 1*D*). This led us to consider whether increased excitability is not related to taste identity or palatability (Wang et al., 2018), but the perceived salience of taste experiences, which encompasses both novelty and valence (Ventura et al., 2007; Kargl et al., 2020). Previous studies have suggested that the induction of plasticity signaling cascades and IEGs in pyramidal neurons of the aIC (commonly used as surrogates for changes in excitability), is a crucial step for the association of taste and visceral information during CTA learning (Adaikkan and Rosenblum, 2015; Soto et al., 2017; Y. Wu et al., 2020). Activation of the aIC-BLA projection is indeed necessary for the expression of neophobia toward saccharin (Kayyal et al., 2021), as well as for CTA learning and retrieval (Kayyal et al., 2019). Yet, its chemogenetic inhibition does not affect the attenuation of neophobia, nor the expression of aversion toward innately aversive quinine (Kayyal et al., 2019). Furthermore, aversive taste memory retrieval necessitates increases in presynaptic inhibitory input on the projection (Yiannakas et al., 2021). Bearing this in mind, we hypothesized that increases in excitability on the projection could be indicative of a labile state of the taste trace at the aIC, which manifests when taste cues are not (yet) highly predictive of the visceral outcome of the sensory experience (Bekisz et al., 2010; Galliano et al., 2021). In such a scenario, taste memory retrieval following strong single-trial aversive learning would be expected to result in decreased excitability compared with control animals. To assess this hypothesis, we next examined intrinsic excitability in mice retrieving an appetitive (Saccharin 2x, CTA Retrieval control) or learned aversive memory (CTA Retrieval) for saccharin.

Learned aversive taste memory retrieval decreases the excitability of LIV–VI aIC-BLA projecting neurons

Following recovery from rAAV injection, mice in the CTA Retrieval group underwent water restriction and CTA conditioning for 0.5% saccharin (see Materials and Methods; Fig. 2*A*). Electrophysiological recordings were obtained from aIC-BLA neurons 3 d later, 1 h following retrieval ($n = 8$ animals, 27 cells). Mice in the Saccharin 2x group on the other hand, were familiarized with saccharin without conditioning, and recordings were obtained within the same period, following retrieval ($n = 5$ animals, 20 cells).

Table 1: Summary of LI–III aIC-BLA intrinsic properties

Groups	RMP (mV)	mAHP (mV)	Input resistance (MΩ)	Sag ratio (%)	Time constant (ms)	AP thresh (mV)	AP Amp (mV)	AP half-width (ms)	Rheobase (pA)
LI–III aIC-BLA Water	−70.84 ± 1.09 (14)	−2.411 ± 0.6767 (14)	136.4 ± 16.85 (14)	3.172 ± 1.082 (14)	11.17 ± 1.169 (14)	−31.35 ± 1.547 (14)	56 ± 1.719 (14)	0.6557 ± 0.03222 (14)	140.7 ± 31.83 (14)
LI–III aIC-BLA Saccharin 1x	−72.27 ± 1.212 (15)	−1.752 ± 0.4953 (15)	131.6 ± 13.14 (15)	3.997 ± 0.9166 (15)	11.56 ± 1.672 (15)	−31.44 ± 1.621 (15)	56.33 ± 1.323 (15)	0.684 ± 0.02767 (15)	136.1 ± 26.44 (15)
LI–III aIC-BLA Saccharin 2x	−73.44 ± 1.295 (15)	−2.165 ± 0.684 (15)	142.5 ± 13.17 (15)	5.793 ± 1.449 (15)	18.63 ± 1.9 (15)	−31.47 ± 2.511 (15)	49.76 ± 2.065 (15)	0.564 ± 0.03708 (15)	104.7 ± 25.03 (15)
LI–III aIC-BLA CTA Retrieval	−72 ± 1.117 (17)	−3.087 ± 2.914 (17)	171.1 ± 22.28 (17)	6.307 ± 1.368 (17)	18.94 ± 1.667 (17)	−34.24 ± 1.445 (17)	48.58 ± 1.472 (17)	0.5518 ± 0.02698 (17)	114.3 ± 31.57 (17)

Values are expressed as mean ± SEM. The number of cells is in parentheses. Statistical analysis was performed by Student's *t* test. RMP, resting membrane potential; mAHP, medium after hyperpolarization potentials; AP Thresh, action potential threshold; AP Amp, action potential amplitude; AP half-width, action potential half-width.

Table 2: Summary of LIV–VI aIC-BLA intrinsic properties

Groups	RMP (mV)	fAHP (mV)	mAHP (mV)	sAHP (mV)	Input resistance (MΩ)	Sag ratio (%)	Time constant (ms)	AP threshold (mV)	AP amplitude (mV)	AP half-width (ms)	Rheobase (pA)
LIV–VI aIC-BLA Cage Control	−68.28 ± 0.8506 (19)	9.191 ± 1.449 (19)**##	−3.73 ± 0.4241 (19)	−1.881 ± 0.3376 (19)	120.7 ± 7.686 (19)	12.41 ± 1.938 (19)	15.03 ± 1.376 (19)	−30.76 ± 2.139 (19)	56.28 ± 0.8818 (19)^^	0.6774 ± 0.03816 (19)	87.47 ± 9.127 (19)
LIV–VI aIC-BLA Water	−69.3 ± 0.9051 (23)	8.15 ± 0.8288 (23)**	−5.535 ± 0.6754 (23)	−3.277 ± 0.4603 (23)	139.1 ± 9.021 (23)	8.909 ± 1.306 (23)	19.24 ± 1.62 (23)	−31.05 ± 1.30 (23)	52.43 ± 1.034 (23)	0.6243 ± 0.02021 (23)	85 ± 11.76 (23)
LIV–VI aIC-BLA Saccharin 1x	−69.21 ± 0.94 (20)	3.016 ± 0.9423 (20)####	−4.17 ± 0.4542 (20)	−2.521 ± 0.2735 (20)	145.8 ± 12.56 (20)	10.89 ± 1.621 (20)	14.82 ± 1.485 (20)#	−30.9 ± 2.141 (20)	52.03 ± 1.308 (20)	0.6005 ± 0.0326 (20)	74.25 ± 11.39 (20)
LIV–VI aIC-BLA Quinine 1x	−67.32 ± 1.092 (19)	13.56 ± 1.562 (19)$$$$~	−5.858 ± 0.5613 (18)	−3.634 ± 0.3632 (18)	146 ± 9.094 (19)	12.13 ± 1.23 (19)	21.55 ± 1.638 (19)	−29.74 ± 1.989 (19)	57.11 ± 1.376 (19)*^^^	0.6 ± 0.03555 (19)	69.89 ± 8.932 (19)
LIV–VI aIC-BLA Saccharin 5x	−66.53 ± 1.358 (18)	8.158 ± 1.356 (18)**###	−3.999 ± 0.653 (18)	−2.695 ± 0.5083 (18)	144.6 ± 14.68 (18)	9.392 ± 2.127 (18)	17.3 ± 1.66 (18)	−32.66 ± 1.783 (18)	56.48 ± 1.337 (18)	0.6539 ± 0.04814 (18)	78.61 ± 10.75 (18)
LIV–VI aIC-BLA Saccharin 1x (4 h)	−69.47 ± 0.7569 (17)	5.989 ± 1.074 (17)**	−4.411 ± 0.8962 (17)	−2.631 ± 0.6949 (17)	153.9 ± 11.10 (17)	10.97 ± 1.475 (17)	26.21 ± 2.421 (17)***$$$%&&	−31.03 ± 1.511 (17)	52.24 ± 2.311 (17)	0.7765 ± 0.03641 (17)**	78.88 ± 9.274 (17)
LIV–VI aIC-BLA Saccharin 2x	−70.79 ± 1.242 (20)	5.223 ± 0.8217 (20)###	−5.301 ± 0.7863 (20)	−3.351 ± 0.3798 (20)	181.1 ± 11.7 (20)	7.815 ± 1.176 (20)	19.28 ± 1.837 (20)	−32.85 ± 1.447 (20)	49.14 ± 1.568 (20)###	0.578 ± 0.02994 (20)	69.6 ± 10.71 (20)
LIV–VI aIC-BLA CTA Retrieval	−68.78 ± 0.8419 (27)	7.97 ± 1.018 (27)##	−5.213 ± 0.4544 (27)	−2.69 ± 0.3064 (27)	136.4 ± 9.064 (27)^^	13.41 ± 1.31 (27)^^	20.96 ± 1.724 (27)*	−31.61 ± 2.68 (27)	56.21 ± 0.9978 (27)^^^	0.5959 ± 0.0208 (27)	90.44 ± 17.56 (27)
LIV–VI aIC-BLA Extinction	−65.98 ± 1.457 (14)	4.731 ± 1.021 (14)	−5.076 ± 0.6981 (14)	−2.895 ± 0.6547 (14)	151.1 ± 15.63 (14)	12.37 ± 1.471 (14)	17.55 ± 2.684 (14)~	−36.06 ± 1.481 (14)~	55.09 ± 2.122 (14)^	0.7386 ± 0.03145 (14)	69.21 ± 7.454 (14)
LIV–VI aIC-BLA Reinstatement	−68.57 ± 0.936 (15)	5.932 ± 1.292 (15)	−5.673 ± 0.4288 (15)	−3.612 ± 0.3033 (15)	178.7 ± 12.1 (15)	9.245 ± 0.884 (15)	25.48 ± 1.58 (15)**	−29.43 ± 1.731 (15)	53.1 ± 2.906 (15)	0.8187 ± 0.06929 (15)	67.6 ± 8.753 (15)

Values are expressed in mean ± SEM. The number of cells is in parentheses. Statistical analysis was performed by one-way ANOVA *post hoc* Tukey's and Dunn's multiple comparisons. Student's *t* test was performed for the comparison between two groups. RMP, resting membrane potential; fAHP, mAHP and sAHP, fast, medium, and slow after hyperpolarization potentials, respectively; AP Thresh, action potential threshold; AP Amp, action potential amplitude; AP half-width, action potential half-width. Data are shown as mean ± SEM *$p < 0.05$, **$p < 0.01$, ***$p < 0.001$, ****$p < 0.0001$, with respect to the corresponding symbols.
$Vs. Cage Control *Vs. Saccharin 1x ^Vs. Saccharin 2x ~Vs. Reinstatement.
%Vs. Water #Vs. Quinine 1x &Vs. Saccharin 5x.

Through this approach we aimed to examine the hypothesis that like innately aversive and highly familiar appetitive responses (Fig. 1), learned aversive taste memory retrieval would be correlated with suppression of the intrinsic excitability on the projection.

As expected, CTA Retrieval mice, exhibited decreased consumption of the conditioned tastant compared with control animals that were only familiarized with saccharin (Fig. 2*B*, Mann–Whitney test, $p = 0.0085$; Sum of ranks: 52.50, 38.50; Mann–Whitney $U = 2.500$). Intrinsic excitability in LIV–VI aIC-BLA projecting neurons was increased in response to depolarizing current injections (Fig. 2*D*; $p < 0.0001$, $F_{(8,360)} = 483.3$), and was significantly different between the two treatments ($p = 0.0014$, $F_{(1,45)} = 11.60$). Excitability was enhanced in the Saccharin 2x group compared with CTA Retrieval, while a significant interaction was identified between the treatment and current injection factors ($p < 0.0001$, $F_{(8,360)} = 9.398$). Fast AHP (fAHP) on LIV–VI aIC-BLA projecting neurons tended to be increased in the CTA Retrieval group (Table 2), however differences compared with Saccharin 2x failed to reach significance (unpaired *t* test; $p = 0.0527$, $t = 1.990$, df = 45). Conversely, AP amplitude in the Saccharin 2x group was significantly decreased compared with CTA Retrieval (Fig. 2*G*; Unpaired *t* test; $p = 0.0002$, $t = 3.983$, df = 45). In addition, the CTA Retrieval group exhibited significantly decreased IR (Fig. 2*H*; unpaired *t* test; $p = 0.0036$, $t = 3.072$, df = 45) and significantly enhanced SAG ratio (Fig. 2*I*; unpaired *t* test; $p = 0.0037$, $t = 3.060$, df = 45), compared with Saccharin 2x. In accord with our hypothesis, excitability on LIV–VI aIC-BLA projecting neurons was decreased by aversive taste memory retrieval. We have previously shown that compared with CTA Retrieval and Reinstatement, appetitive memory retrieval and extinction were associated with (1) an enhancement of IEG induction (c-fos and Npas4) at the aIC, and (2) decreased frequency of presynaptic inhibition on the aIC-BLA (Yiannakas et al., 2021). In accord, other published work investigating the induction of IEG in the rodent IC, found that consistent with a reduction in spiking activity (Grossman et al., 2008), the induction of c-fos in IC neurons was decreased by aversive taste memory retrieval (Haley et al., 2020). Earlier studies have also reported increases in c-fos following the extinction of cyclosporine A-induced CTA (Hadamitzky et al.,

Table 3: Summary of BS LIV–VI aIC-BLA intrinsic properties

Groups	RMP (mV)	fAHP (mV)	mAHP (mV)	sAHP (mV)	Input resistance (MΩ)	Sag ratio (%)	Time constant (ms)	AP thresh (mV)	AP Amp (mV)	AP half-width (ms)	Rheobase (pA)
BS LIV–VI aIC-BLA Cage Control	−68.28 ± 0.9705 (13)	9.192 ± 2.061 (13)	−4.194 ± 0.5072 (13)	−2.075 ± 0.4500 (13)	118.4 ± 9.771 (13)	14.91 ± 2.195 (13)	14.71 ± 1.944 (13)	−31.83 ± 2.971 (13)	56.27 ± 1.147 (13)	0.6692 ± 0.05460 (13)	74.54 ± 8.471 (13)
BS LIV–VI aIC-BLA Water	−69.00 ± 1.639 (11)	7.800 ± 1.607(11)	−4.870 ± 0.8838 (11)	−2.826 ± 0.6069 (11)	136.5 ± 14.40 (11)	8.751 ± 2.021 (11)	18.03 ± 2.309 (11)	−29.27 ± 2.060 (11)	54.21 ± 1.572 (11)	0.6736 ± 0.03111 (11)	85.91 ± 13.44 (11)
BS LIV–VI aIC-BLA Saccharin 1x	−68.80 ± 1.065 (17)	2.870 ± 1.044 (17)	−4.339 ± 0.5083 (17)	−2.564 ± 0.3032 (17)	146.6 ± 14.22 (17)	11.67 ± 1.790 (17)	14.27 ± 1.666 (17)	−30.73 ± 2.385 (17)	51.64 ± 1.473 (17)	0.5976 ± 0.03555 (17)	63.65 ± 7.679 (17)
BS LIV–VI aIC-BLA Quinine 1x	−67.37 ± 1.682 (9)	13.67 ± 2.681(9) ##	−6.131 ± 0.6514 (8)	−3.58 ± 0.5788 (8)	139.2 ± 16.86 (9)	14.15 ± 2.159 (9)	23.21 ± 2.717 (9)	−29.35 ± 3.071 (9)	58.86 ± 2.003 (9)	0.6378 ± 0.0491 (9)	59.56 ± 12.28 (9)
BS LIV–VI aIC-BLA Saccharin 5x	−67.20 ± 1.624 (10)	11.30 ± 1.727 (10) ##	−5.174 ± 0.8427 (10)	−3.609 ± 0.7205 (10)	156.1 ± 22.85 (10)	11.92 ± 3.395 (10)	17.11 ± 2.296 (10)	−30.38 ± 2.493 (10)	58.40 ± 1.812 (10)	0.7140 ± 0.07349 (10)	76.60 ± 15.32 (10)
BS LIV–VI aIC-BLA Saccharin 1x (4 h)	−68.20 ± 1.293 (6)	3.433 ± 0.9245(6)	−6.693 ± 1.442 (6)	−3.130 ± 1.637 (6)	154.9 ± 22.41(6)	14.99 ± 2.770 (6)	26.09 ± 5.331 (6)	−34.61 ± 2.174 (6)	46.79 ± 4.359 (6)	0.8850 ± 0.05943 (6) #	60.83 ± 11.36 (6)
BS LIV–VI aIC-BLA Saccharin 2x	−71.33 ± 1.641 (13)	4.169 ± 0.9225 (13)	−5.368 ± 0.9616 (13)	−3.226 ± 0.4899 (13)	180.3 ± 15.15 (13) **	7.017 ± 1.317 (13) ***	19.77 ± 2.447 (13)	−34.20 ± 1.987 (13)	46.18 ± 1.666 (13) ***	0.5331 ± 0.03522 (13)	77.54 ± 15.69 (13)
BS LIV–VI aIC-BLA CTA Retrieval	−67.37 ± 1.21 (12)	5.473 ± 1.464 (12)	−4.633 ± 0.5831 (12)	−1.932 ± 0.4462 (12)	110.9 ± 12.98 (12)	16.8 ± 1.869 (12)	17.06 ± 2.608 (12)	−34.28 ± 1.771 (12)	57.87 ± 1.678 (12)	0.6367 ± 0.03961 (12)	88.75 ± 9.847 (12)
BS LIV–VI aIC-BLA Extinction	−67.36 ± 1.43 (11)	3.943 ± 1.111 (11)	−4.816 ± 0.8447 (11)	−2.104 ± 0.4466 (11) ~	131.1 ± 13.93 (11)	13.69 ± 1.541 (11)	14.52 ± 2.714 (11) ~ ~	−37.41 ± 1.636 (11) ~ ~	57.3 ± 2.023 (11)	0.7155 ± 0.03674 (11)	81 ± 6.932 (11)
BS LIV–VI aIC-BLA Reinstatement	−68.88 ± 1.163 (10)	6.432 ± 1.737 (10)	−5.243 ± 0.5853 (10)	−3.804 ± 1.339 (10)	157.4 ± 10.56 (10)	9.124 ± 1.03 (10)	26.93 ± 1.893 (10)	−27.5 ± 2.195 (10)	57.36 ± 3.001 (10)	0.769 ± 0.03494 (10)	73.9 ± 12.45 (10)

Values are expressed in mean ± SEM. The number of cells is in parentheses. Statistical analysis was performed by one-way ANOVA *post hoc* Tukey's and Dunn's multiple comparisons. Student's *t* test was performed for the comparison between two groups. RMP, resting membrane potential; fAHP, mAHP, and sAHP, fast, medium, and slow after hyperpolarization potentials, respectively; AP Thresh, action potential threshold; AP Amp, action potential amplitude; AP half-width, action potential half-width.
*BS LV/VI aIC-BLA Saccharin 2x vs. CTA Retrieval, *$p < 0.05$, **$p < 0.01$, ***$p < 0.001$.
~BS LV/VI aIC-BLA Extinction vs. Reinstatement, ~$p < 0.05$, ~~$p < 0.01$, ~~~$p < 0.001$.
#BS LV/VI aIC-BLA Saccharin 1x vs. Quinine 1x, Saccharin 5x and Saccharin 1x (4hr), #$p < 0.05$, ##$p < 0.01$.

2015). We thus hypothesized that if excitability in these cells serves as key node for a change in valence prediction, extinction, which constitutes a form of appetitive re-learning, would be associated with enhanced excitability compared with CTA Retrieval and reinstatement (Berman, 2003; Suzuki et al., 2004; Morrison et al., 2016; Slouzkey and Maroun, 2016). In addition, through these extinction and reinstatement studies, we were able to examine the real-life relevance of these changes on intrinsic excitability, in a context where behavioral performance reflects the balance between contrasting memories and the availability of retrieval cues (Fig. 3).

The predictability of the valence arising from taste experiences determines the profile of intrinsic properties of LIV–VI aIC-BLA projecting neurons

Using similar approaches, electrophysiological recordings were obtained from LIV–VI aIC-BLA projecting neurons from mice having undergone unreinforced CTA extinction (Extinction; $n = 5$, 14 cells), or US-mediated CTA reinstatement (Reinstatement; $n = 3$ animals, 15 cells). Behaviorally, the two groups of animals were similar in terms of their aversion profile over 9 unreinforced extinction sessions (Fig. 3*B*; two-way ANOVA; Extinction: $p < 0.0001$, $F_{(8,54)} = 13.44$; Treatment: $p = 0.0681$, $F_{(1,54)} = 3.466$; Interaction: $p = 0.9697$, $F_{(8,54)} = 0.2803$). As expected, saccharin consumption during the test day in the Reinstatement group was decreased compared with Extinction (Fig. 3C; Mann–Whitney test; $p = 0.0179$; Sum or ranks: 30, 6; Mann–Whitney $U = 0$). Consistent with our findings in Figure 2, aversive taste memory retrieval in the Reinstatement group was associated with decreased excitability compared with the Extinction group (Fig. 3*E*; two-way ANOVA, Current injection: $p < 0.0001$, $F_{(8,216)} = 370.1$; Treatment: $p = 0.0297$, $F_{(1,27)} = 5.291$; Interaction: $p < 0.0001$, $F_{(8,216)} = 10.30$). CTA Reinstatement was also associated with increases in the AP threshold (Fig. 3*F*; unpaired *t* test: $p = 0.0076$, $t = 2.887$, df = 27) and τ (Fig. 3*G*; unpaired *t* test: $p = 0.0153$, $t = 2.589$, df = 27) compared with Extinction.

Unlike animals that underwent familiarization with the tastant without conditioning (Fig. 1), excitability on the projection in the Extinction group was not decreased

Table 4: Summary of RS LIV–VI aIC-BLA intrinsic properties

Groups	RMP (mV)	fAHP (mV)	mAHP (mV)	sAHP (mV)	Input resistance (MΩ)	Sag ratio (%)	Time constant (ms)	AP thresh (mV)	AP Amp (mV)	AP half-width (ms)	Rheobase (pA)
RS LIV–VI aIC-BLA Cage Control	−68.29 ±1.830 (6)	9.188 ± 1.351 (6)	−2.725 ± 0.6462 (6)	−1.460 ± 0.4409 (6)	125.7 ± 13.03 (6)	6.993 ± 3.030 (6)	15.73 ± 1.333 (6)	−28.44 ± 2.166 (6)	56.30 ± 1.422 (6)	0.6950 ± 0.03170 (6)	115.5 ± 18.62 (6)
RS LIV–VI aIC-BLA Water	−69.57 ± 0.9422 (12)	8.472 ± 0.6792 (12)	−6.144 ± 1.013 (12)	−3.690 ± 0.6876 (12)	141.5 ±11.75 (12)	9.735 ± 1.400 (12)	20.35 ± 2.321 (12)	−32.67 ± 1.561 (12)	50.79 ± 1.238 (12)	0.5792 ± 0.01928 (12)	84.17 ± 19.48 (12)
RS LIV–VI aIC-BLA Saccharin 1x	−71.57 ± 1.120 (3)	3.840 ± 2.530 (3)	−3.210 ± 0.9005 (3)	−2.277 ± 0.7297 (3)	141.3 ±28.45 (3)	6.455 ± 3.099 (3)	17.95 ± 2.856 (3)	−31.86 ± 5.650 (3)	54.23 ± 2.660 (3)	0.6167 ± 0.09939 (3)	134.3 ± 58.52 (3)
RS LIV–VI aIC-BLA Quinine 1x	−67.28 ±1.505 (10)	11.63 ± 1.616 (10)	−5.639 ± 0.8918 (10)	−3.678 ± 0.4895 (10)	151.4 ± 9.055 (10)	10.31 ± 1.115 (10)	23.6 ± 1.77(10)	−30.1 ± 2.732 (10)	55.53 ± 1.845 (10)	0.6230 ± 0.0535 (10)	79.20 ± 12.73 (10)
RS LIV–VI aIC-BLA Saccharin 5x	−65.70 ± 2.378 (8)	4.235 ± 1.141 (8)	−2.530 ± 0.7960 (8)	−1.553 ±0.4915 (8)	130.1 ± 16.85 (8)	6.237 ± 1.910 (8)	17.54 ± 2.561 (8)	−35.50 ± 2.302 (8)	54.09 ± 1.734 (8)	0.5788 ± 0.05034 (8)	81.13 ±15.88 (8)
RS LIV–VI aIC-BLA Saccharin 1x (4 h)	−70.17 ± 0.9075 (11)	7.383 ± 1.439 (11)	−3.165 ± 0.9897 (11)	−2.359 ± 0.6647 (11)	153.3 ± 12.96 (11)	8.782 ± 1.389 (11)	26.28 ± 2.596 (11)	−28.43 ± 1.652 (11)	51.66 ± 3.053 (11)	0.7773 ± 0.04702 (11)	88.73 ± 12.25 (11)
RS LIV–VI aIC-BLA Saccharin 2x	−69.79 ± 1.921 (7)	7.180 ± 1.402 (7)	−5.016 ± 1.460 (7)	−3.581 ± 0.6324 (7)	182.6 ± 19.62 (7)	9.297 ± 2.347 (7)	18.36 ± 2.842 (7)	−30.36 ± 1.638 (7)	54.62 ± 2.058 (7)	0.6614 ± 0.04149 (7)	54.86 ± 8.207 (7)
RS LIV–VI aIC-BLA CTA Retrieval	−69.9 ± 1.116 (15)	9.967 ± 1.216 (15)	−5.667 ± 0.6647 (15)	−3.297 ± 0.3599(15)	156.7 ± 10.11 (15)	10.71 ± 1.536 (15)	24.08 ± 2.023 (15)	−33.9 ± 1.132 (15)	54.89 ± 1.13 (15)	0.5633 ± 0.01703 (15) *	91.8 ± 31.15 (15)
RS LIV–VI aIC-BLA Extinction	−60.93 ± 3.263 (3)	7.620 ± 1.907 (3)	−6.027 ± 1.062 (3)	−5.797 ± 1.997 (3)	224.2 ± 21.29 (3)	7.515 ± 2.666 (3)	28.69 ± 2.138 (3)	−31.1 ± 1.372 (3)	46.98 ± 4.432 (3)	0.8233 ± 0.02603 (3)	36.67 ± 13.33 (3)
RS LIV–VI aIC-BLA Reinstatement	−67.95 ± 1.725 (5)	4.932 ± 1.893 (5)	−6.532 ± 0.3344 (5)	−3.228 ± 0.3214 (5)	221.2 ± 18.9 (5)	9.486 ± 1.846 (5)	22.58 ± 2.632 (5)	−33.31 ± 2.035 (5)	44.58 ± 4.569 (5)	0.918 ± 0.203 (5)	55 ± 6.885 (5)

Values are expressed in mean ± SEM. The number of cells is in parentheses. Statistical analysis was performed by One-way ANOVA *post hoc* Tukey's and Dunn's multiple comparisons. Student's *t* test was performed for the comparison of two groups. RMP, resting membrane potential; fAHP, mAHP, and sAHP, fast, medium, and slow after hyperpolarization potentials, respectively; AP Thresh, action potential threshold; AP Amp, action potential amplitude; AP half-width, action potential half-width.
*RS LV/VI aIC-BLA Saccharin 1x vs. CTA Retrieval, *$p < 0.05$.

by familiarization (Fig. 3). Conversely, although the intrinsic mechanisms employed would appear to differ, aversive taste memory retrieval regardless of prior experience, was associated with baseline excitability of the aIC-BLA projection (Fig. 3). Our findings in this section (Fig. 3), revealed that during taste memory retrieval, excitability on the projection is not solely dependent on the relevant novelty or appetitive nature of tastants, and does not subserve the persistence of CTA memories (Fig. 2). Instead, excitability on the aIC-BLA projection is indeed shaped by prior experience but is best predicted by the probability for further aversive (re)learning.

Next, to distinguish between intrinsic properties changes that reproducibly reflect taste identity, familiarity, and valence over the course of time and experience, we compared the profile of intrinsic properties across pairs of behavioral groups in which the currently perceived novelty, as well as innate or learned valence associated with taste was notably different. Through this comparison we were led to conclude that excitability on aIC-BLA projecting neurons is driven by taste stimuli of positive valence, however this effect is dependent on subjective experience and the possibility for further associative learning (Fig. 4*A*). Excitability on aIC-BLA projecting neurons in the treatment groups where the tastant was perceived as appetitive (Saccharin 1x, Saccharin 2x, and Extinction), was closely matched, and was significantly enhanced compared with the innately or learned aversive (Quinine 1x, CTA Retrieval, and Reinstatement) groups (Fig. 4*A*; two-way ANOVA; Current injection: $p < 0.0001$, $F_{(5,872)} = 1218$; Treatment: $p = 0.0014$, $F_{(5,109)} = 4.281$; Interaction: $p < 0.0001$, $F_{(40,872)} = 4.978$). As previously identified in Figure 1*H*, fAHP reflected the innate aversive nature of the tastant, being increased in the Quinine 1x group compared with all other groups (Fig. 4*B*; one-way ANOVA; $F = 10.65$, $p < 0.0001$, $R^2 = 0.3283$; see Table 2). Significant differences in IR (Fig. 4*C*; one-way ANOVA; $F = 2.775$, $p = 0.0213$, $R^2 = 0.1129$) and SAG ratio (Fig. 4*D*; one-way ANOVA; $F = 2.610$, $p = 0.0286$, $R^2 = 0.1069$) were only observed between the CTA Retrieval and Saccharin 2x groups. AP amplitude (Fig. 4*E*; one-way ANOVA, $p = 0.0054$, $F = 3.526$, $R^2 = 0.1392$) in the Saccharin 2x group was decreased compared with both CTA Retrieval ($p = 0.0129$, q = 4.768, df = 109) and Quinine 1x ($p = 0.0087$, q = 4.944, df = 109). Conversely, the Extinction and Reinstatement groups, where familiarity with the tastant was the highest, exhibited

Table 5: Statistics table

Figure	Statistical test	Results
Figure 1		
Figure 1*B*	One -Way Anova Water consumption the before the test Water Saccharin 1x Quinine 1x Saccharin 5x Saccharin 1x (4hrs)	ANOVA results: F = 0.9766 P = 0.4424 R squared, 0.1634

Figure 1*D*	Two-way repeated measures ANOVA
	Post-hoc Tukey's multiple comparisons
	LIV-VI aIC-BLA neurons
	F-I curve
	Cage control
	Water
	Saccharin 1x
	Quinine 1x
	Saccharin 5x
	Saccharin 1x (4hr)
		ANOVA Results:
		Treatment; p = 0.0057, F (5, 110) = 3.491
		Current; p < 0.0001, F (8, 880) = 1276
		Interaction; p < 0.0001, F (40, 880) = 4.141
		Multiple Comparisons:
		0pA
		Cage control vs. Water
		Mean difference = 0.000
		Cage control vs. Saccharin 1x
		Mean difference = 0.000
		Cage control vs. Quinine 1x
		Mean difference = 0.000
		Cage Control vs. Saccharin 5x
		Mean difference = 0.000
		Cage Control vs. Saccharin 1x (4hr)
		Mean difference = 0.000
		Water vs. Saccharin 1x
		Mean difference = 0.000
		Water vs. Quinine 1x
		Mean difference = 0.000
		Water vs. Saccharin 5x
		Mean difference = 0.000
		Water vs. Saccharin 1x (4hr)
		Mean difference = 0.000
		Saccharin 1x vs. Quinine 1x
		Mean difference = 0.000
		Saccharin 1x vs. Saccharin 5x
		Mean difference = 0.000
		Saccharin 1x vs. Saccharin 1x (4hr)
		Mean difference = 0.000
		Quinine 1x vs. Saccharin 5x
		Mean difference = 0.000
		Quinine 1x vs. Saccharin 1x (4hr)
		Mean difference = 0.000
		Saccharin 5x vs. Saccharin 1x (4hr)
		Mean difference = 0.000
		50pA
		Cage control vs. Water
		p = 0.9902, q = 0.8645, df = 990.0;
		Cage control vs. Saccharin 1x
		p = 0.9993, q = 0.5005, df = 990.0;
		Cage Control vs. Quinine 1x
		p >0.9999, q = 0.2597, df = 990.00;
		Cage control vs. Saccharin 5x
		p = 0.9451, q = 1.281, df = 990.00;
		Cage control vs. Saccharin 1x(4hr)
		p = 0.9922, q = 0.8240, df = 990;
		Water vs. Saccharin 1x
		p = 0.9999, q = 0.3522, df = 990
		Water vs. Quinine 1x
		p = 0.9946, q = 0.5927, df = 990;
		Water vs. Saccharin 5x
		p = 0.9984, q = 0.4868, df = 990;
		Water vs. Saccharin 1x (4hr)

(Continued)

Table 5: Continued

Figure	Statistical test	Results

		p>0.9999, q = 0.02212, df = 990;
		Saccharin 1x vs. Quinine 1x
		p>0.9999, q = 0.2374, df = 990;
		Saccharin 1x vs. Saccharin 5x
		p = 0.9931, q = 0.8029, df = 990;
		Saccharin 1x vs. Saccharin 1x (4hr)
		p = 0.9999, q = 0.3478, df = 990;
		Quinine 1x vs. Saccharin 5x
		p = 0.9790, q = 1.024, df = 990;
		Quinine 1x vs. Saccharin 1x (4hr)
		p = 0.9986, q = 0.5716, df = 990;
		Saccharin 5x vs. Saccharin 1x (4hr)
		p = 0.9996, q = 0.4320, df = 990;
		100pA
		Cage control vs. Water
		p = 0.8652, q = 1.610, df = 990.0;
		Cage control vs. Saccharin 1x
		p = 0.2233, q = 3.159, df = 990.0;
		Cage Control vs. Quinine 1x
		p = 0.4580, q = 2.563, df = 990.00;
		Cage control vs. Saccharin 5x
		p = 0.6454, q = 2.163, df = 990.00;
		Cage control vs. Saccharin 1x(4hr)
		p = 0.5930, q = 2.275, df = 990;
		Water vs. Saccharin 1x
		p = 0.8437, q = 1.677, df = 990
		Water vs. Quinine 1x
		p = 0.9742, q = 1.073, df = 990;
		Water vs. Saccharin 5x
		p = 0.9969, q = 0.6743, df = 990;
		Water vs. Saccharin 1x (4hr)
		p = 0.9926, q = 0.8138, df = 990;
		Saccharin 1x vs. Quinine 1x
		p = 0.9987, q = 0.5625, df = 990;
		Saccharin 1x vs. Saccharin 5x
		p = 0.9867, q = 0.9250, df = 990;
		Saccharin 1x vs. Saccharin 1x (4hr)
		p = 0.9945, q = 0.7652, df = 990;
		Quinine 1x vs. Saccharin 5x
		p = 0.9998, q = 0.3658, df = 990;
		Quinine 1x vs. Saccharin 1x (4hr)
		p>0.9999, q = 0.2164, df = 990;
		Saccharin 5x vs. Saccharin 1x (4hr)
		p>0.9999, q = 0.1422, df = 990;
		150pA
		Cage control vs. Water
		p = 0.8024, q = 1.793, df = 990.0;
		Cage control vs. Saccharin 1x
		p = 0.0085, q = 4.836, df = 990.0;
		Cage Control vs. Quinine 1x
		p = 0.1482, q = 3.431, df = 990.00;
		Cage control vs. Saccharin 5x
		p = 0.2881, q = 2.970, df = 990.00;
		Cage control vs. Saccharin 1x(4hr)
		p = 0.5463, q = 2.374, df = 990;
		Water vs. Saccharin 1x
		p = 0.1962, q = 3.248, df = 990
		Water vs. Quinine 1x
		p = 0.8009, q = 1.797, df = 990;
		Water vs. Saccharin 5x
		p = 0.9345, q = 1.337, df = 990;
		Water vs. Saccharin 1x (4hr)

(Continued)

Table 5: Continued

Figure	Statistical test	Results

		p = 0.9953, q = 0.7397, df = 990;
		Saccharin 1x vs. Quinine 1x
		p = 0.9297, q = 1.361, df = 990;
		Saccharin 1x vs. Saccharin 5x
		p = 0.8142, q = 1.762, df = 990;
		Saccharin 1x vs. Saccharin 1x (4hr)
		p = 0.5843, q = 2.293, df = 990;
		Quinine 1x vs. Saccharin 5x
		p = 0.9997, q = 0.4145, df = 990;
		Quinine 1x vs. Saccharin 1x (4hr)
		p = 0.9843, q = 0. 0.9603, df = 990;
		Saccharin 5x vs. Saccharin 1x (4hr)
		P = 0.9989, q = 0.5448, df = 990;
		200pA
		Cage Control vs. Water
		p = 0.9968, q = 0.6822, df = 990.0;
		Cage Control vs. Saccharin 1x
		p = 0.0038, q = 0.6822, df = 990.0;
		Cage Control vs. Quinine 1x
		p = 0.5360, q = 2.396, df = 990.0;
		Cage Control vs. Saccharin 5x
		p = 0.5556, q = 2.354, df = 990.0;
		Cage Control vs. Saccharin 1x (4hr)
		p = 0.9876, q = 0.9108, df = 990.0;
		Water vs. Saccharin 1x
		p = 0.0116, q = 4.708, df = 990.0;
		Water vs. Quinine 1x
		p = 0.7904, q = 4.708, df = 990.0;
		Water vs. Saccharin 5x
		p = 0.8042, q = 1.789, df = 990.0;
		Water vs. Saccharin 1x (4hr)
		p>0.9999, q = 0.2894, df = 990.0;
		Saccharin 1x vs. Quinine 1x
		p = 0.3853, q = 2.727, df = 990.0;
		Saccharin 1x vs. Saccharin 5x
		p = 0.3979, q = 2.698, df = 990.0;
		Saccharin 1x vs. Saccharin 1x (4hr)
		p = 0.0457, q = 4.083, df = 990.0;
		Quinine 1x vs. Saccharin 5x
		p>0.9999, q = 0.008880, df = 990.0;
		Quinine 1x vs. Saccharin 1x (4hr)
		p = 0.9172, q = 1.417, df = 990.0;
		Saccharin 5x vs. Saccharin 1x (4hr)
		p = 0.9233, q = 1.391, df = 990.0;
		250pA
		Cage control vs. Water
		p = 0.9988, q = ,0.5590 df = 990.0;
		Cage control vs. Saccharin 1x
		p = 0.0011, q = 5.603, df = 990.0;
		Cage Control vs. Quinine 1x
		p = 0.7555, q = 1.912, df = 990.0;
		Cage Control vs. Saccharin 5x
		p = 0.7478, q = 1.931, df = 990.0;
		Cage Control vs. Saccharin 1x (4hr)
		p>0.9999, q = 0.1164, df = 990.0;
		Water vs. Saccharin 1x
		p = 0.0026, q = 5.304, df = 990.0;
		Water vs. Quinine 1x
		p = 0.9113, q = 1.442, df = 990.0;
		Water vs. Saccharin 5x
		p = 0.9051, q = 1.468, df = 990.0;
		Water vs. Saccharin 1x (4hr)

(Continued)

Table 5: Continued

Figure	Statistical test	Results

		p = 0.9972, q = 0.6633, df = 990.0;
		Saccharin 1x vs. Quinine 1x
		p = 0.1000, q = 3.666, df = 990.0;
		Saccharin 1x vs. Saccharin 5x
		p = 0.1180, q = 3.570, df = 990.0;
		Saccharin 1x vs. Saccharin 1x (4hr)
		p = 0.0013, q = 5.559, df = 990.0;
		Quinine 1x vs. Saccharin 5x
		p>0.9999, q = 0.04456, df = 990.0;
		Quinine 1x vs. Saccharin 1x (4hr)
		p = 0.7292, q = 1.975, df = 990.0;
		Saccharin 5x vs. Saccharin 1x (4hr)
		p = 0.7215, q = 1.993, df = 990.0;
		300pA
		Cage Control vs. Water
		p = 0.9993, q = 0.4987, df = 990.0;
		Cage Control vs. Saccharin 1x
		p = 0.0005, q = 5.903, df = 990.0;
		Cage Control vs. Quinine 1x
		p = 0.9022, q = 1.479, df = 990.0;
		Cage Control vs. Saccharin 5x
		p = 0.7419, q = 1.945, df = 990.0;
		Cage Control vs. Saccharin 1x (4hr)
		p = 0.9641, q = 1.158, df = 990.0;
		Water vs. Saccharin 1x
		p = 0.0009, q = 5.679, df = 990.0;
		Water vs. Quinine 1x
		p = 0.9766, q = 1.049, df = 990.0;
		Water vs. Saccharin 5x
		p = 0.8854, q = 1.542, df = 990.0;
		Water vs. Saccharin 1x (4hr)
		p = 0.8386, q = 1.692, df = 990.0;
		Saccharin 1x vs. Quinine 1x
		p = 0.0232, q = 4.405, df = 990.0;
		Saccharin 1x vs. Saccharin 5x
		p = 0.0716, q = 3.851, df = 990.0;
		Saccharin 1x vs. Saccharin 1x (4hr)
		p < 0.0001, q = 6.905, df = 990.0;
		Quinine 1x vs. Saccharin 5x
		p = .9994, q = 0.4860, df = 990.0;
		Quinine 1x vs. Saccharin 1x (4hr)
		p = 0.4433, q = 2.596, df = 990.0;
		Saccharin 5x vs. Saccharin 1x (4hr)
		p = 0.2645, q = 3.035, df = 990.0;
		350pA
		Cage Control vs. Water
		p = 0.9973, q = 0.6556, df = 990.0;
		Cage Control vs. Saccharin 1x
		p = 0.0003, q = 6.069, df = 990.0;
		Cage Control vs. Quinine 1x
		p = 0.9972, q = 0.6596, df = 990.0;
		Cage Control vs. Saccharin 5x
		p = 0.8294, q = 1.719, df = 990.0;
		Cage Control vs. Saccharin 1x (4hr)
		p = 0.7347, q = 1.962, df = 990.0;
		Water vs. Saccharin 1x
		p = 0.0009, q = 5.694, df = 990.0;
		Water vs. Quinine 1x
		p>0.9999, q = 0.03478, df = 990.0;
		Water vs. Saccharin 5x
		p = 0.9650, q = 1.151, df = 990.0;
		Water vs. Saccharin 1x (4hr)

(Continued)

Table 5: Continued

Figure	Statistical test	Results

		p = 0.4043, q = 2.683, df = 990.0;
		Saccharin 1x vs. Quinine 1x
		p = 0.0020, q = 5.401, df = 990.0;
		Saccharin 1x vs. Saccharin 5x
		p = 0.0328, q = 4.244, df = 990.0;
		Saccharin 1x vs. Saccharin 1x (4hr)
		p < 0.0001, q = 7.879, df = 990.0;
		Quinine 1x vs. Saccharin 5x
		p = 0.9747, q = 1.068, df = 990.0;
		Quinine 1x vs. Saccharin 1x (4hr)
		p = 0.4400, q = 2.603, df = 990.0;
		Saccharin 5x vs. Saccharin 1x (4hr)
		p = 0.1105, q = 3.609, df = 990.0;
		400pA
		Cage Control vs. Water
		p = 0.9988, q = 0.5513, df = 990.0;
		Cage Control vs. Saccharin 1x
		p = 0.0004, q = 5.939, df = 990.0;
		Cage Control vs. Quinine 1x
		p = 0.9987, q = 0.5623, df = 990.0;
		Cage Control vs. Saccharin 5x
		p = 0.9132, q = 1.435, df = 990.0;
		Cage Control vs. Saccharin 1x (4hr)
		p = 0.3765, q = 2.748, df = 990.0;
		Water vs. Saccharin 1x
		p = 0.0009, q = 5.663, df = 990.0;
		Water vs. Quinine 1x
		p>0.9999, q = 0.03710, df = 990.0;
		Water vs. Saccharin 5x
		p = 0.9845, q = 0.9564, df = 990.0;
		Water vs. Saccharin 1x (4hr)
		p = 0.1551, q = 3.402, df = 990.0;
		Saccharin 1x vs. Quinine 1x
		p = 0.0021, q = 5.369, df = 990.0;
		Saccharin 1x vs. Saccharin 5x
		p = 0.0233, q = 4.403, df = 990.0;
		Saccharin 1x vs. Saccharin 1x (4hr)
		p < 0.0001, q = 8.548, df = 990.0;
		Quinine 1x vs. Saccharin 5x
		p = 0.9894, q = 0.8800, df = 990.0;
		Quinine 1x vs. Saccharin 1x (4hr)
		p = 0.1832, q = 3.294, df = 990.0;
		Saccharin 5x vs. Saccharin 1x (4hr)
		p = 0.0435, q = 4.108, df = 990.0.

Figure 1*H*	One-way ANOVA
	Kruskal-Wallis test
	Post-hoc Dunn's multiple comparisons test
	LIV-VI aIC-BLA neurons
	fAHP
	Cage control
	Water
	Saccharin 1x
	Quinine 1x
	Saccharin 5x
	Saccharin 1x (4hr)
		ANOVA results:
		Kruskal-Wallis test, p < 0.0001;
		Kruskal-Wallis statistic, 29.91.
		Multiple Comparisons:
		Cage Control vs. Water
		p >0.9999, z = 0.2306;
		Cage Control vs. Saccharin 1x
		p = 0.0136, z = 3.318;
		Cage Control vs. Quinine 1x
		p >0.9999, z = 1.809;
		Cage Control vs. Saccharin 5x
		p >0.9999, z = 0.4824;
		Cage Control vs. Saccharin 1x (4hr)
		p>0.9999, z = 1.648;
		Water vs. Saccharin 1x
		p = 0.0177, z = 3.243;
		Water vs. Quinine 1x
		p = 0.5054, z = 2.124;

(Continued)

Table 5: Continued

Figure	Statistical test	Results

		Water vs. Saccharin 5x
		p>0.9999, z = 0.2771;
		Water vs. Saccharin 1x (4hr)
		p>0.9999, z = 1.497;
		Saccharin 1x vs. Quinine 1x
		p < 0.0001, z = 5.150;
		Saccharin 1x vs. Saccharin 5x
		p = 0.0807, z = 2.783;
		Saccharin 1x vs. Saccharin 1x (4hr)
		p>0.9999, z = 1.554;
		Quinine 1x vs. Saccharin 5x
		p = 0.3511 z = 2.267;
		Quinine 1x vs. Saccharin 1x (4hr)
		p = 0.0099, z = 3.406;
		Saccharin 5x vs. Saccharin 1x (4hr)
		p>0.9999, z = 1.1583

Figure 1*I*	One-way ANOVA
	Kruskal-Wallis test
	Post-hoc Dunn's multiple comparisons test
	LIV-VI aIC-BLA neurons
	Action Potential Half-width
	Cage control
	Water
	Saccharin 1x
	Quinine 1x
	Saccharin 5x
	Saccharin 1x (4hr)
		ANOVA results:
		Kruskal-Wallis test, p = 0.0125; Kruskal-Wallis statistic,14.54.
		Multiple Comparisons:
		Cage Control vs. Water
		p >0.9999, z = 0.7692;
		Cage Control vs. Saccharin 1x
		p>0.9999, z = 1.627;
		Cage Control vs. Quinine 1x
		p >0.9999, z = 0.9868 ;
		Cage Control vs. Saccharin 5x
		p >0.9999, z = 0.6540;
		Cage Control vs. Saccharin 1x (4hr)
		P = 0.8292, z = 1.917;
		Water vs. Saccharin 1x
		p >0.9999, z = 0.9244;
		Water vs. Quinine 1x
		p>0.9999, z = 0.2636;
		Water vs. Saccharin 5x
		p>0.9999, z = 0.07420;
		Water vs. Saccharin 1x (4hr)
		p = 0.0905, z = 2.746;
		Saccharin 1x vs. Quinine 1x
		p>0.9999, z = 0.6271
		Saccharin 1x vs. Saccharin 5x
		p = >0.9999, z = 0.9418;
		Saccharin 1x vs. Saccharin 1x (4hr)
		p = 0.0065, z = 3.519;
		Quinine 1x vs. Saccharin 5x
		p>0.9999z = 0.3194;
		Quinine 1x vs. Saccharin 1x (4hr)
		p = 0.0605, z = 2.876;
		Saccharin 5x vs. Saccharin 1x (4hr)
		p = 0.1721, z = 2.528

Figure 1*J*	One-way ANOVA
	Post-hoc Tukey's multiple comparisons
	LIV-VI aIC-BLA neurons
	Membrane Time Constant
	Cage control
	Water
	Saccharin 1x
	Quinine 1x
	Saccharin 5x
	Saccharin 1x (4hr)
		ANOVA results:
		Treatment; p < 0.0001, F (5, 110) = 6.094;
		R squared, 0.2169;
		Multiple Comparisons:
		Cage Control vs. Water
		p = 0.4608, q = 2.566, df = 110;
		Cage Control vs. Saccharin 1x
		p >0.9999, q = 0.1233, df = 110;
		Cage Control vs. Quinine 1x
		p = 0.0864, q = 3.798, df = 110;
		Cage Control vs. Saccharin 5x
		p = 0.9398, q = 1.306, df = 110;

(Continued)

Table 5: Continued

Figure	Statistical test	Results

		Cage Control vs. Saccharin 1x (4hr)
		p = 0.0003, q = 6.326, df = 110;
		Water vs. Saccharin 1x
		p = 0.3890, q = 2.731, df = 110;
		Water vs. Quinine 1x
		p = 0.9184, q = 1.408, df = 110;
		Water vs. Saccharin 5x
		p = 0.9628, q = 1.163, df = 110;
		Water vs. Saccharin 1x (4hr)
		p = 0.0488, q = 4.115, df = 110;
		Saccharin 1x vs. Quinine 1x
		p = 0.0639, q = 3.969, df = 110;
		Saccharin 1x vs. Saccharin 5x
		p = 0.9101, q = 1.443, df = 110;
		Saccharin 1x vs. Saccharin 1x (4hr)
		p = 0.0002, q = 6.521, df = 110;
		Quinine 1x vs. Saccharin 5x
		p = 0.5180, q = 2.440, df = 110;
		Quinine 1x vs. Saccharin 1x (4hr)
		p = 0.4302, q = 2.635, df = 110;
		Saccharin 5x vs. Saccharin 1x (4hr)
		p = 0.0081, q = 4.975, df = 110;

Figure 2		
Figure 2*B*	Two-tailed Unpaired t-test Saccharin consumption on the test day Saccharin 2x CTA retrieval	t-test Results: Mann-Whitney test, p = 0.0085, Mann-Whitney U, 2.500

Figure 2*D*	Two-way repeated measures ANOVA
	Post-hoc Šídák's multiple comparisons test
	LIV-VI aIC-BLA neurons
	F-I curve
	Saccharin 2x
	CTA retrieval
		ANOVA Results:
		Treatment; $p < 0.0014$, F (1, 45) = 11.60
		Current; $p < 0.0001$, F (8, 360) = 483.3
		Interaction; $p < 0.0001$, F (8, 360) = 9.398
		Multiple Comparisons:
		0pA
		Saccharin 2x vs. CTA retrieval
		Mean difference = 0.000
		50pA
		Saccharin 2x vs. CTA retrieval
		p>0.9999, t = 0.1045, df = 405.0;
		100pA
		Saccharin 2x vs. CTA retrieval
		p = 0.5860, t = 1.682, df = 405.0;
		150pA
		Saccharin 2x vs. CTA retrieval
		p = 0.0286, t = 2.964, df = 405.0;
		200pA
		Saccharin 2x vs. CTA retrieval
		p = 0.0019, t = 3.738, df = 405.0;
		250pA
		Saccharin 2x vs. CTA retrieval
		p = 0.0005, t = 4.090, df = 405.0;
		300pA
		Saccharin 2x vs. CTA retrieval
		p = 0.0002, t = 4.280, df = 405.0;
		350pA
		Saccharin 2x vs. CTA retrieval
		$p < 0.0001$, t = 4.517, df = 405.0;
		400pA
		Saccharin 2x vs. CTA retrieval
		p = 0.0003, t = 4.161, df = 405.0

Figure 2*G*	Two-tailed Unpaired t-test LIV-VI aIC-BLA neurons Action Potential Amplitude	t-test Results: p = 0.0002 t = 3.983

(Continued)

Table 5: Continued

Figure	Statistical test	Results
	Saccharin 2x	df = 45
	CTA retrieval	Difference between means = 7.080±1.777
		R squared, 0.2607
Figure 2*H*	Two-tailed Unpaired t-test	t-test Results:
	LIV-VI aIC-BLA neurons	p = 0.0036
	Input Resistance	t = 3.072
	Saccharin 2x	df = 45
	CTA retrieval	Difference between means = 44.75±14.57
		R squared = 0.1734
Figure 2*I*	Two-tailed Unpaired t-test	t-test Results:
	LIV-VI aIC-BLA neurons	p = 0.0037
	SAG Ratio	t = 3.060
	Saccharin 2x	df = 45
	CTA retrieval	Difference between means = 5.597±1.829
		R squared = 0.1723
Figure 3		
Figure 3*B*	Two-way ANOVA	ANOVA Results:
	Post-hoc Šídák's multiple comparisons test	Treatment, P = 0.068, F (1, 54) = 3.466;
		Interaction, P = 0.9697, F (8, 54) = 0.2803.
Figure 3*C*	Two-tailed Unpaired t-test	t-test Results:
	Saccharin consumption on the test day	Mann-Whitney test, p = 0.0179;
	Extinction	Mann-Whitney U, 0
	Reinstatement	
Figure 3*E*	Two-way repeated measures ANOVA	ANOVA Results:
	Post-hoc Šídák's multiple comparisons test	Treatment; p = 0.0013, F (3, 72) = 5.837
	LIV-VI aIC-BLA neurons	Current; p < 0.0001, F (1.959, 141.0) = 802.5
	F-I curve	Interaction; p < 0.0001, F (24, 567) = 6.468
		Multiple Comparisons:
		0pA
		Extinction vs. Reinstatement
		Mean difference = 0.000;
		50pA
		Extinction vs. Reinstatement
		p >0.9999, t = 0.1718, df = 243.0;
		100pA
		Extinction vs. Reinstatement
		p = 0.8899, t = 1.237, df = 243.0;
		150pA
		Extinction vs. Reinstatement
		p >0.9999, t = 0.2492, df = 243.0;
		200pA
		Extinction vs. Reinstatement
		p = 0.5553, t = 1.723, df = 243.0;
		250pA
		Extinction vs. Reinstatement
		p = 0.0341, t = 2.919, df = 243.0;
		300pA
		Extinction vs. Reinstatement
		p = 0.0030, t = 3.636, df = 243.0;
		350pA
		Extinction vs. Reinstatement
		p = 0.0003, q = 4.203, df = 243.0;
		400pA
		Extinction vs. Reinstatement
		p < 0.0001, t = 4.578, df = 243.0.
Figure 3*F*	Two-tailed Unpaired t-test	t-test Results:
	LIV-VI aIC-BLA neurons	p = 0.0076
	Action Potential Threshold	t = 2.887
	Extinction	df = 27
	Reinstatement	Difference between means; 6.621 ± 2.293
		R squared, 0.2359

(Continued)

Table 5: Continued

Figure	Statistical test	Results
Figure 3*G*	Two-tailed Unpaired t-test LIV-VI aIC-BLA neurons Membrane Time Constant Extinction Reinstatement	t-test Results: p = 0.0153 t = 2.589 df = 27 Difference between means ;7.931 ± 3.064 R squared; 0.1988
Figure 4		

Figure 4*A*	Two-way repeated measures ANOVA
	Post-hoc Tukey's multiple comparisons
	LIV-VI aIC-BLA neurons
	F-I Curve
	Saccharin 1x
	Quinine 1x
	Saccharin 2x
	CTA retrieval
	Extinction
	Reinstatement
		ANOVA results:
		Treatment; p = 0.0014, F (5, 109) = 4.281
		Current; p < 0.0001, F (1.990, 216.9) = 1218
		Interaction; p < 0.0001, F (40, 872) = 4.978
		Multiple Comparisons:
		0pA
		Saccharin 1x vs. Quinine 1x
		Mean difference = 0.000
		Saccharin 1x vs. Saccharin 2x
		Mean difference = 0.000
		Saccharin 1x vs. CTA Retrieval
		Mean difference = 0.000
		Saccharin 1x vs. Extinction
		Mean difference = 0.000
		Saccharin 1x vs. Reinstatement
		Mean difference = 0.000
		Quinine 1x vs. Saccharin 2x
		Mean difference = 0.000
		Quinine 1x vs. CTA Retrieval
		Mean difference = 0.000
		Quinine 1x vs. Extinction
		Mean difference = 0.000
		Quinine 1x vs. Reinstatement
		Mean difference = 0.000
		Saccharin 2x vs. CTA Retrieval
		Mean difference = 0.000
		Saccharin 2x vs. Extinction
		Mean difference = 0.000
		Saccharin 2x vs. Reinstatement
		Mean difference = 0.000
		CTA Retrieval vs. Extinction
		Mean difference = 0.000
		CTA Retrieval vs. Reinstatement
		Mean difference = 0.000
		Extinction vs. Reinstatement
		Mean difference = 0.000
		50pA
		Saccharin 1x vs. Quinine 1x
		p>0.9999q = 0.2195, df = 981.0;
		Saccharin 1x vs. Saccharin 2x
		p = 0.9993, q = 0.5023, df = 981.0;
		Saccharin 1x vs. CTA Retrieval
		p = 0.9998, q = 0.3831, df = 981.0;
		Saccharin 1x vs. Extinction
		p = 0.9986, q = 0.5691, df = 981.0;
		Saccharin 1x vs. Reinstatement
		p = 0.9999q = 0.3539, df = 981.0;
		Quinine 1x vs. Saccharin 2x
		p = 0.9960, q = 0.7153, df = 981.0;
		Quinine 1x vs. CTA Retrieval
		p = 0.9981, q = 0.6123, df = 981.0;
		Quinine 1x vs. Extinction
		p = 0.9945, q = 0.7626, df = 981.0;
		Quinine 1x vs. Reinstatement
		p = 0.9988, q = 0.5535, df = 981.0;

(Continued)

Table 5: Continued

Figure	Statistical test	Results

		Saccharin 2x vs. CTA Retrieval
		p>0.9999, q = 0.1553, df = 981.0;
		Saccharin 2x vs. Extinction
		p>0.9999, q = 0.1132, df = 981.0;
		Saccharin 2x vs. Reinstatement
		p>0.9999, q = 0.1112, df = 981.0;
		CTA Retrieval vs. Extinction
		p>0.9999, q = 0.2589, df = 981.0;
		CTA Retrieval vs. Reinstatement
		p>0.9999, q = 0.02435, df = 981.0;
		Extinction vs. Reinstatement
		p>0.9999, q = 0.2084, df = 981.0;
		100pA
		Saccharin 1x vs. Quinine 1x
		p = 0.9991, q = 0.5199, df = 981.0;
		Saccharin 1x vs. Saccharin 2x
		p = 0.8659, q = 1.608, df = 981.0;
		Saccharin 1x vs. CTA Retrieval
		p = 0.9941, q = 0.7759, df = 981.0;
		Saccharin 1x vs. Extinction
		p = 0.9933, q = 0.7975, df = 981.0;
		Saccharin 1x vs. Reinstatement
		p = 0.9924, q = 0.8188, df = 981.0;
		Quinine 1x vs. Saccharin 2x
		p = 0.6709, q = 2.107, df = 981.0;
		Quinine 1x vs. CTA Retrieval
		p >0.9999, q = 0.2082, df = 981.0;
		Quinine 1x vs. Extinction
		p >0.9999, q = 0.3161, df = 981.0;
		Quinine 1x vs. Reinstatement
		p = 0.9431, q = 1.292, df = 981.0;
		Saccharin 2x vs. CTA Retrieval
		p = 0.4875, q = 2.499, df = 981.0;
		Saccharin 2x vs. Extinction
		p = 0.6016, q = 2.257, df = 981.0;
		Saccharin 2x vs. Reinstatement
		p = 0.9970, q = 0.6698, df = 981.0;
		CTA Retrieval vs. Extinction
		p >0.9999, q = 0.1487, df = 981.0;
		CTA Retrieval vs. Reinstatement
		p = 0.8745, q = 1.579, df = 981.0;
		Extinction vs. Reinstatement
		p = 0.8967, q = 1.500, df = 981.0
		150pA
		Saccharin 1x vs. Quinine 1x
		p = 0.9491, q = 1.258, df = 981.0;
		Saccharin 1x vs. Saccharin 2x
		p = 0.8741, q = 1.258, df = 981.0;
		Saccharin 1x vs. CTA Retrieval
		p = 0.3926, q = 2.71, df = 981.0;
		Saccharin 1x vs. Extinction
		p>0.9999, q = 0.2459, df = 981.0;
		Saccharin 1x vs. Reinstatement
		p = 0.9985, q = 0.5798, df = 981.0;
		Quinine 1x vs. Saccharin 2x
		p = 0.5798, q = 2.818, df = 981.0;
		Quinine 1x vs. CTA Retrieval
		p = 0.937, q = 1.324, df = 981.0;
		Quinine 1x vs. Extinction
		p = 0.9882, q = 0.9008, df = 981.0;
		Quinine 1x vs. Reinstatement
		p = 0.9983, q = 0.5934, df = 981.0;

(Continued)

Table 5: Continued

Figure	Statistical test	Results

		Saccharin 2x vs. CTA Retrieval
		p = 0.0233, q = 4.404, df = 981.0;
		Saccharin 2x vs. Extinction
		p = 0.8426, q = 0.8426, df = 981.0;
		Saccharin 2x vs. Reinstatement
		p = 0.6995, q = 0.6995, df = 981.0;
		CTA Retrieval vs. Extinction
		p = 0.6431, q = 2.168, df = 981.0;
		CTA Retrieval vs. Reinstatement
		p = 0.7735, q = 1.868, df = 981.0;
		Extinction vs. Reinstatement
		p>0.9999, q = 0.3023, df = 981.0
		200pA
		Saccharin 1x vs. Quinine 1x
		p = 0.4777, q = 2.521, df = 981.0;
		Saccharin 1x vs. Saccharin 2x
		p = 0.9511, q = 1.246, df = 981.0;
		Saccharin 1x vs. CTA Retrieval
		p = 0.0346, q = 4.219, df = 981.0;
		Saccharin 1x vs. Extinction
		p>0.9999, q = 0.07085, df = 981.0;
		Saccharin 1x vs. Reinstatement
		p = 0.627, q = 2.202, df = 981.0;
		Quinine 1x vs. Saccharin 2x
		p = 0.0862, q = 3.75, df = 981.0;
		Quinine 1x vs. CTA Retrieval
		p = 0.907, q = 1.46, df = 981.0;
		Quinine 1x vs. Extinction
		p = 0.5516, q = 2.363, df = 981.0;
		Quinine 1x vs. Reinstatement
		p>0.9999, q = 0.1599, df = 981.0;
		Saccharin 2x vs. CTA Retrieval
		p = 0.0013, q = 5.554, df = 981.0;
		Saccharin 2x vs. Extinction
		p = 0.9756, q = 1.06, df = 981.0;
		Saccharin 2x vs. Reinstatement
		p = 0.1668, q = 3.356, df = 981.0;
		CTA Retrieval vs. Extinction
		p = 0.0712, q = 3.854, df = 981.0;
		CTA Retrieval vs. Reinstatement
		p = 0.8889, q = 1.529, df = 981.0;
		Extinction vs. Reinstatement
		p = 0.6782, q = 2.091, df = 981.0
		250pA
		Saccharin 1x vs. Quinine 1x
		p = 0.1585, q = 3.389, df = 981.0;
		Saccharin 1x vs. Saccharin 2x
		p = 0.9907, q = 0.8555, df = 981.0;
		Saccharin 1x vs. CTA Retrieval
		p = 0.0038, q = 5.16, df = 981.0;
		Saccharin 1x vs. Extinction
		p >0.9999, q = 0.3001, df = 981.0;
		Saccharin 1x vs. Reinstatement
		p = 0.1227, q = 3.547, df = 981.0;
		Quinine 1x vs. Saccharin 2x
		p = 0.0336, q = 4.233, df = 981.0;
		Quinine 1x vs. CTA Retrieval
		p = 0.9074, q = 1.459, df = 981.0;
		Quinine 1x vs. Extinction
		p = 0.1609, q = 3.379, df = 981.0;
		Quinine 1x vs. Reinstatement
		p = 0.9998, q = 0.3641, df = 981.0;

(Continued)

Table 5: Continued

Figure	Statistical test	Results

		Saccharin 2x vs. CTA Retrieval
		p = 0.0003, q = 6.078, df = 981.0;
		Saccharin 2x vs. Extinction
		p = 0.9994, q = 0.4763, df = 981.0;
		Saccharin 2x vs. Reinstatement
		p = 0.0268, q = 4.339, df = 981.0;
		CTA Retrieval vs. Extinction
		p = 0.0066, q = 4.94, df = 981.0;
		CTA Retrieval vs. Reinstatement
		p = 0.9838, q = 0.9659, df = 981.0;
		Extinction vs. Reinstatement
		p = 0.1238, q = 3.541, df = 981.0
		300pA
		Saccharin 1x vs. Quinine 1x
		p = 0.0468, q = 4.071, df = 981.0;
		Saccharin 1x vs. Saccharin 2x
		p = 0.9991, q = 0.5264, df = 981.0;
		Saccharin 1x vs. CTA Retrieval
		p = 0.0006, q = 5.795, df = 981.0;
		Saccharin 1x vs. Extinction
		p = 0.9998, q = 0.3808, df = 981.0;
		Saccharin 1x vs. Reinstatement
		p = 0.023, q = 4.41, df = 981.0;
		Quinine 1x vs. Saccharin 2x
		p = 0.0153, q = 4.591, df = 981.0;
		Quinine 1x vs. CTA Retrieval
		p = 0.9311, q = 1.354, df = 981.0;
		Quinine 1x vs. Extinction
		p = 0.046, q = 4.08, df = 981.0;
		Quinine 1x vs. Reinstatement
		p = 0.9985, q = 0.585, df = 981.0;
		Saccharin 2x vs. CTA Retrieval
		p = 0.0001, q = 6.36, df = 981.0;
		Saccharin 2x vs. Extinction
		p >0.9999, q = 0.09689, df = 981.0;
		Saccharin 2x vs. Reinstatement
		p = 0.0073, q = 4.898, df = 981.0;
		CTA Retrieval vs. Extinction
		p = 0.0011, q = 5.594, df = 981.0;
		CTA Retrieval vs. Reinstatement
		p = 0.9978, q = 0.6315, df = 981.0;
		Extinction vs. Reinstatement
		p = 0.0229, q = 4.411, df = 981.0
		350pA
		Saccharin 1x vs. Quinine 1x
		p = 0.0058, q = 4.992, df = 981.0;
		Saccharin 1x vs. Saccharin 2x
		p = 0.9998, q = 0.4001, df = 981.0;
		Saccharin 1x vs. CTA Retrieval
		p = 0.0001, q = 6.284, df = 981.0;
		Saccharin 1x vs. Extinction
		p >0.9999, q = 0.2699, df = 981.0;
		Saccharin 1x vs. Reinstatement
		p = 0.0028, q = 5.272, df = 981.0;
		Quinine 1x vs. Saccharin 2x
		p = 0.0021, q = 5.387, df = 981.0;
		Quinine 1x vs. CTA Retrieval
		p = 0.9909, q = 0.8504, df = 981.0;
		Quinine 1x vs. Extinction
		p = 0.0092, q = 4.807, df = 981.0;
		Quinine 1x vs. Reinstatement
		p = 0.9985, q = 0.5836, df = 981.0;

(Continued)

Table 5: Continued

Figure	Statistical test	Results

		Saccharin 2x vs. CTA Retrieval
		p < 0.0001, q = 6.713, df = 981.0;
		Saccharin 2x vs. Extinction
		p >0.9999, q = 0.09312, df = 981.0;
		Saccharin 2x vs. Reinstatement
		p = 0.001, q = 5.642, df = 981.0;
		CTA Retrieval vs. Extinction
		p = 0.0005, q = 5.914, df = 981.0;
		CTA Retrieval vs. Reinstatement
		p >0.9999, q = 0.1648, df = 981.0;
		Extinction vs. Reinstatement
		p = 0.0044, q = 5.099, df = 981.0
		400pA
		Saccharin 1x vs. Quinine 1x
		p = 0.0062, q = 4.963, df = 981.0;
		Saccharin 1x vs. Saccharin 2x
		p >0.9999, q = 0.24, df = 981.0;
		Saccharin 1x vs. CTA Retrieval
		p = 0.0004, q = 5.925, df = 981.0;
		Saccharin 1x vs. Extinction
		p = 0.9991, q = 0.5192, df = 981.0;
		Saccharin 1x vs. Reinstatement
		p = 0.0014, q = 5.513, df = 981.0;
		Quinine 1x vs. Saccharin 2x
		p = 0.0034, q = 5.2, df = 981.0;
		Quinine 1x vs. CTA Retrieval
		p = 0.9991, q = 0.5284, df = 981.0;
		Quinine 1x vs. Extinction
		p = 0.0053, q = 5.027, df = 981.0;
		Quinine 1x vs. Reinstatement
		p = 0.991, q = 0.8492, df = 981.0;
		Saccharin 2x vs. CTA Retrieval
		p = 0.0002, q = 6.183, df = 981.0;
		Saccharin 2x vs. Extinction
		p >0.9999, q = 0.3014, df = 981.0;
		Saccharin 2x vs. Reinstatement
		p = 0.0008, q = 5.736, df = 981.0;
		CTA Retrieval vs. Extinction
		p = 0.0005, q = 5.857, df = 981.0;
		CTA Retrieval vs. Reinstatement
		p = 0.9997, q = 0.4195, df = 981.0;
		Extinction vs. Reinstatement
		p = 0.0013, q = 5.554, df = 981.0

Figure 4*B*	One-way ANOVA
	Post-hoc Tukey's multiple comparisons
	LIV-VI aIC-BLA neurons
	fAHP
	Saccharin 1x
	Quinine 1x
	Saccharin 2x
	CTA retrieval
	Extinction
	Reinstatement
		ANOVA results:
		Treatment; p < 0.0001, F (5, 109) = 10.64;
		R squared, 0.3283;
		Multiple Comparisons:
		Saccharin 1x vs. Quinine 1x
		p < 0.0001, q = 9.380, df = 109;
		Saccharin 1x vs. Saccharin 2x
		p = 0.7249, q = 1.985, df = 109;
		Saccharin 1x vs. CTA Retrieval
		p = 0.0127, q = 4.774, df = 109;
		Saccharin 1x vs. Extinction
		p = 0.9204, q = 1.399, df = 109;
		Saccharin 1x vs. Reinstatement
		p = 0.5239, q = 2.428, df = 109;
		Quinine 1x vs. Saccharin 2x
		p < 0.0001, q = 7.421, df = 109;
		Quinine 1x vs. CTA Retrieval
		p = 0.0035, q = 5.331, df = 109;
		Quinine 1x vs. Extinction

(Continued)

Table 5: Continued

Figure	Statistical test	Results

		p < 0.0001, q = 7.147, df = 109;
		Quinine 1x vs. Reinstatement
		p = 0.0003, q = 6.299, df = 109;
		Saccharin 2x vs. CTA Retrieval
		p = 0.4251, q = 2.647, df = 109;
		Saccharin 2x vs. Extinction
		p = 0.9997, q = 0.4017, df = 109;
		Saccharin 2x vs. Reinstatement
		p = 0.9983, q = 0.5902, df = 109;
		CTA Retrieval vs. Extinction
		p = 0.3621, q = 2.796, df = 109;
		CTA Retrieval vs. Reinstatement
		p = 0.7995, q = 1.799, df = 109;
		Extinction vs. Reinstatement
		p = 0.9868, q = 0.9191, df = 109.

Figure 4*C*	One-way ANOVA
	Post-hoc Tukey's multiple comparisons
	LIV-VI aIC-BLA neurons
	Input Resistance
	Saccharin 1x
	Quinine 1x
	Saccharin 2x
	CTA retrieval
	Extinction
	Reinstatement
		ANOVA results:
		Treatment; p = 0.0213, F (5, 109) = 2.775;
		R squared, 0.1129;
		Multiple Comparisons:
		Saccharin 1x vs. Quinine 1x
		p >0.9999, q = 0.03668, df = 109;
		Saccharin 1x vs. Saccharin 2x
		p = 0.2331, q = 3.152, df = 109;
		Saccharin 1x vs. CTA Retrieval
		p = 0.9876, q = 0.9065, df = 109;
		Saccharin 1x vs. Extinction
		p = 0.9997, q = 0.4256, df = 109;
		Saccharin 1x vs. Reinstatement
		p = 0.3953, q = 2.716, df = 109;
		Quinine 1x vs. Saccharin 2x
		p = 0.2582, q = 3.075, df = 109;
		Quinine 1x vs. CTA Retrieval
		p = 0.9859, q = 0.9323, df = 109;
		Quinine 1x vs. Extinction
		p = 0.9998, q = 0.3877, df = 109;
		Quinine 1x vs. Reinstatement
		p = 0.4229, q = 2.652, df = 109;
		Saccharin 2x vs. CTA Retrieval
		p = 0.0352, q = 4.286, df = 109;
		Saccharin 2x vs. Extinction
		p = 0.5204, q = 2.435, df = 109;
		Saccharin 2x vs. Reinstatement
		p >0.9999, q = 0.2024, df = 109;
		CTA Retrieval vs. Extinction
		p = 0.9475, q = 1.262, df = 109;
		CTA Retrieval vs. Reinstatement
		p = 0.1001, q = 3.711, df = 109;
		Extinction vs. Reinstatement
		p = 0.6757, q = 2.098, df = 109.

Figure 4*D*	One-way ANOVA
	Post-hoc Tukey's multiple comparisons
	LIV-VI aIC-BLA neurons
	Sag ratio
	Saccharin 1x
	Quinine 1x
	Saccharin 2x
	CTA retrieval
	Extinction
	Reinstatement
		ANOVA results:
		Treatment; p = 0.0286, F (5, 109) = 2.610;
		R squared, 0.1069;
		Multiple Comparisons:
		Saccharin 1x vs. Quinine 1x
		p = 0.9862, q = 0.9280, df = 109;
		Saccharin 1x vs. Saccharin 2x
		p = 0.5707, q = 2.327, df = 109;
		Saccharin 1x vs. CTA Retrieval
		p = 0.6972, q = 2.049, df = 109;
		Saccharin 1x vs. Extinction
		p = 0.9794, q = 1.015, df = 109;
		Saccharin 1x vs. Reinstatement

(Continued)

Table 5: Continued

Figure	Statistical test	Results

		p = 0.9643, q = 1.152, df = 109;
		Quinine 1x vs. Saccharin 2x
		p = 0.2112, q = 3.225, df = 109;
		Quinine 1x vs. CTA Retrieval
		p = 0.9784, q = 1.026, df = 109;
		Quinine 1x vs. Extinction
		p>0.9999, q = 0.1598, df = 109;
		Quinine 1x vs. Reinstatement
		p = 0.7184, q = 2.000, df = 109;
		Saccharin 2x vs. CTA Retrieval
		p = 0.0209, q = 4.543, df = 109;
		Saccharin 2x vs. Extinction
		p = 0.2415, q = 3.126, df = 109;
		Saccharin 2x vs. Reinstatement
		p = 0.9805q = 1.002, df = 109;
		CTA Retrieval vs. Extinction
		p = 0.9944, q = 0.7617, df = 109;
		CTA Retrieval vs. Reinstatement
		p = 0.2504, q = 3.099, df = 109;
		Extinction vs. Reinstatement
		p = 0.7140, q = 2.010, df = 109.

Figure 4*E*	One-way ANOVA
	Post-hoc Tukey's multiple comparisons
	LIV-VI aIC-BLA neurons
	Action Potential Amplitude
	Saccharin 1x
	Quinine 1x
	Saccharin 2x
	CTA retrieval
	Extinction
	Reinstatement
		ANOVA results:
		Treatment; p = 0.0054, F (5, 109) = 3.526;
		R squared, 0.1392;
		Multiple Comparisons:
		Saccharin 1x vs. Quinine 1x
		p = 0.2342, q = 3.149, df = 109;
		Saccharin 1x vs. Saccharin 2x
		p = 0.7922, q = 1.818, df = 109;
		Saccharin 1x vs. CTA Retrieval
		p = 0.3531, q = 2.818, df = 109;
		Saccharin 1x vs. Extinction
		p = 0.8190, q = 1.746, df = 109;
		Saccharin 1x vs. Reinstatement
		p = 0.9979, q = 0.6222df = 109;
		Quinine 1x vs. Saccharin 2x
		p = 0.0087, q = 4.944, df = 109;
		Quinine 1x vs. CTA Retrieval
		p = 0.9983, q = 0.5921, df = 109;
		Quinine 1x vs. Extinction
		p = 0.9662, q = 1.137, df = 109;
		Quinine 1x vs. Reinstatement
		p = 0.5806, q = 2.305, df = 109;
		Saccharin 2x vs. CTA Retrieval
		p = 0.0129, q = 4.768, df = 109;
		Saccharin 2x vs. Extinction
		p = 0.1650, q = 3.396, df = 109;
		Saccharin 2x vs. Reinstatement
		p = 0.5804, q = 2.306, df = 109;
		CTA Retrieval vs. Extinction
		p = 0.9968, q = 0.6777, df = 109;
		CTA Retrieval vs. Reinstatement
		p = 0.7511, q = 1.922, df = 109;
		Extinction vs. Reinstatement
		p = 0.9746, q = 1.065, df = 109.

Figure 4*F*	One-way ANOVA Kruskal-Wallis test Post-hoc Dunn's multiple comparisons test LIV-VI aIC-BLA neurons Action Potential Half-width Saccharin 1x Quinine 1x	ANOVA results: Kruskal-Wallis test; p = 0.0002; Kruskal-Wallis statistic,24.03 Multiple Comparisons: Saccharin 1x vs. Quinine 1x p >0.9999, z = 0.6106 Saccharin 1x vs. Saccharin 2x p >0.9999, z = 0.2586;

(Continued)

Table 5: Continued

Figure	Statistical test	Results

	Saccharin 2x
	CTA retrieval
	Extinction
	Reinstatement
		Saccharin 1x vs. CTA Retrieval
		p >0.9999, z = 0.04096;
		Saccharin 1x vs. Extinction
		p = 0.0485, z = 2.944;
		Saccharin 1x vs. Reinstatement
		p = 0.0200, z = 3.208;
		Quinine 1x vs. Saccharin 2x
		p >0.9999, q = 0.8658;
		Quinine 1x vs. CTA Retrieval
		p >0.9999, z = 0.6129;
		Quinine 1x vs. Extinction
		p = 0.2759, z = 2.358;
		Quinine 1x vs. Reinstatement
		p = 0.1372, z = 2.607;
		Saccharin 2x vs. CTA Retrieval
		p >0.9999, z = 0.3181;
		Saccharin 2x vs. Extinction
		p = 0.0222, z = 3.179;
		Saccharin 2x vs. Reinstatement
		p = 0.0085, z = 3.448;
		CTA Retrieval vs. Extinction
		p = 0.0312, z = 3.079;
		CTA Retrieval vs. Reinstatement
		p = 0.0115, z = 3.366;
		Extinction vs. Reinstatement
		p >0.9999, z = 0.1880.

Figure 4*G*	One-way ANOVA
	Post-hoc Tukey's multiple comparisons
	LIV-VI aIC-BLA neurons
	Membrane Time Constant
	Saccharin 1x
	Quinine 1x
	Saccharin 2x
	CTA retrieval
	Extinction
	Reinstatement
		ANOVA results:
		Treatment; p = 0.0047, F (5, 109) = 0.1419;
		R squared, 0.1419;
		Multiple Comparisons:
		Saccharin 1x vs. Quinine 1x
		p = 0.0987, q = 3.720, df = 109;
		Saccharin 1x vs. Saccharin 2x
		p = 0.4932, q = 2.495, df = 109;
		Saccharin 1x vs. CTA Retrieval
		p = 0.1046, q = 3.685, df = 109;
		Saccharin 1x vs. Extinction
		p = 0.9230, q = 1.388, df = 109;
		Saccharin 1x vs. Reinstatement
		p = 0.0022, q = 5.525, df = 109;
		Quinine 1x vs. Saccharin 2x
		p = , 0.9484 q = 1.257, df = 109;
		Quinine 1x vs. CTA Retrieval
		p = 0.9999, q = 0.3489, df = 109;
		Quinine 1x vs. Extinction
		p = 0.7139, q = 2.010, df = 109;
		Quinine 1x vs. Reinstatement
		p = 0.7124, q = 2.014, df = 109;
		Saccharin 2x vs. CTA Retrieval
		p = 0.9798, q = 1.011, df = 109;
		Saccharin 2x vs. Extinction
		p = 0.9894, q = 0.8761, df = 109;
		Saccharin 2x vs. Reinstatement
		p = 0.2138, q = 3.216, df = 109;
		CTA Retrieval vs. Extinction
		p = 0.7866, q = 1.833, df = 109;
		CTA Retrieval vs. Reinstatement
		p = 0.4978, q = 2.484, df = 109;
		Extinction vs. Reinstatement
		p = 0.0896, q = 3.777, df = 109.

increased AP half-width compared with all other groups (Fig. 4*F*; one-way ANOVA, Kruskal–Wallis test; $p = 0.0002$; Kruskal–Wallis statistic, 24.03). Significant differences in terms of τ (Fig. 4*G*; one-way ANOVA, $p = 0.0047$, $F = 3.606$) were only observed in comparing the Saccharin 1x and Reinstatement groups ($p = 0.0022$, $q = 5.525$, $df = 109$). Hence, neuronal excitability is indeed a feature associated with predictive power to modulate taste valence, however it does not fully reflect the breadth of intrinsic property changes among the different behavioral groups.

The predictability of taste valence intrinsic is primarily reflected on the excitability of burst spiking, but not regular spiking LIV–VI aIC-BLA projecting neurons

Our initial analysis of individual intrinsic properties (Figs. 1-3) highlighted that excitability is enhanced following appetitive experiences in which the internal representation is still labile and is associated with the possibility for further aversive learning (novelty or extinction). Conversely, following extensive familiarization, aversive conditioning, or reinstatement, whereby taste exposure leads to memory retrieval of specific valence, excitability on LIV–VI aIC-BLA projecting neurons was similar to baseline (Figs. 1, 4). While the precise mechanism through which sensory input is encoded at the cortex (and other key regions), is still a matter of ongoing research, studies indicate that bursting in cortical Layer V pyramidal neurons can encode oscillating currents into a pattern that can be reliably transmitted to distant postsynaptic terminals (Kepecs and Lisman, 2003; Samengo et al., 2013; Zeldenrust et al., 2018). Spike burst is defined as the occurrence of three or more spikes from a single neuron with $<$8-ms intervals (Ranck, 1973; Connors et al., 1982). In brain slices from naive mice, half of the neurons of a given structure exhibit burst firing, while the distribution of burst spiking (BS) to regular spiking (RS) neurons, changes along the anterior-posterior axis of the subiculum (Staff et al., 2000; Jarsky et al., 2008). Importantly, the two cell types fine-tune the output of brain structures by virtue of differences in synaptic plasticity, as well as intrinsic excitability mechanisms (Graves et al., 2012; Song et al., 2012). Furthermore, there are changes in the ratio of BS:RS neurons in individual brain structures, as well as differences in the recruitment of signaling events, ion channels and metabotropic receptors among the two cell types (Wozny et al., 2008; Shor et al., 2009). Correspondingly, complex region and task-specific rules govern the molecular and electrophysiological mechanisms through which information encoding and retrieval takes place in the two cell types (Dunn et al., 2018; Dunn and Kaczorowski, 2019). Little is currently known regarding the influence of cell identity in the repertoire of plasticity mechanisms employed by the IC to facilitate taste-guided behaviors (Maffei et al., 2012; Haley and Maffei, 2018).

Our *post hoc* spike sorting analysis allowed us to distinguish between BS and RS LIV–VI aIC-BLA projecting neurons, and thus their relative contribution to behaviorally driven changes in the suit of intrinsic properties (Extended Data Figs. 1-3, 2-1, 3-1). Through this comparison, we uncovered that Saccharin 1x differed to other groups in terms of excitability and fAHP in BS LIV–VI aIC-BLA neurons (Extended Data Fig. 1-3; Table 3), while no such changes were observed in RS neurons (see summary of RS intrinsic properties; Table 4). Similarly, excitability in the Saccharin 2x group was significantly enhanced compared with CTA Retrieval in BS, but not in RS, LIV–VI aIC-BLA neurons (Extended Data Fig. 2-1*A*,*F*). Significant differences in IR, SAG ratio and AP amplitude between CTA Retrieval and Saccharin 2x were primarily driven by BS LIV–VI aIC-BLA neurons (Extended Data Fig. 2-1*B–D*, *G–I*). Conversely, significant differences in AP half-width between the aversive and appetitive memory retrieval groups were only observed in RS neurons (Extended Data Fig. 2-1*J*). Correspondingly, excitability in the Extinction group was enhanced compared with Reinstatement in BS, and not RS, LIV–VI aIC-BLA neurons (Extended Data Fig. 3-1*A*,*H*). Indeed, excitability on BS LIV–VI aIC-BLA neurons following extinction and reinstatement, reflected the subjective predictability of taste memory retrieval, being high following extinction compared with reinstatement (Extended Data Fig. 3-1). However, this effect was mediated through alternative mechanisms compared with single-trial learning and memory retrieval (Extended Data Figs. 1-3, 2-1, 3-1). Significant differences between the Extinction and Reinstatement groups, were observed in terms of the sAHP, AP threshold, SAG ratio, and τ in BS but not in RS LIV–VI aIC-BLA neurons (Extended Data Fig. 3-1*B–F*).

Encouraged by these findings, we focused on the Saccharin 1x, Saccharin 2x, Saccharin 5x, CTA Retrieval, Extinction, and Reinstatement groups, as to isolate the contribution of BS LIV–VI aIC-BLA neurons in encoding the subjective predictability of taste experience during taste learning, re-learning, and memory retrieval (Fig. 5). Consistent with studies in the hippocampus (Graves et al., 2016), we found that the percentage of BS LIV–VI aIC-BLA projecting neurons in the sampled population was highest in the context of novel taste learning (Extended Data Fig. 1–2*B*; Saccharin 1x, 85%), and subsided following progressive familiarization (Extended Data Fig. 1-2*B*; Saccharin 2x, 65%, Mann–Whitney test: $p = 0.0562$; Sum of ranks: 303.5, 161.5; Mann–Whitney $U = 70.50$; Saccharin 5x, 55.56%, Mann–Whitney test: $p = 0.0034$; Sum of ranks: 291, 87; Mann–Whitney $U = 32$). Interestingly, animals retrieving CTA, exhibited the lowest proportion of BS neurons among the six treatments (Extended Data Fig. 1-2*B*; CTA Retrieval, 44.44% BS), and significant differences were observed compared with control animals (Extended Data Fig. 1-2*B*; Saccharin 2x, 65% BS; Mann–Whitney test: $p = 0.0102$; Sum of ranks: 257, 208; Mann–Whitney $U = 55$). Thus, the ratio of BS:RS LIV–VI aIC-BLA projecting neurons was plastic in relation to experience and was highest in response to appetitive novelty, in accord with studies investigating the intrinsic excitability of subiculum output neurons in relation to contextual novelty and valence encoding (Dunn et al., 2018). Indeed, the ratio of BS:RS LIV–VI aIC-BLA neurons was progressively decreased by familiarity acquisition (Saccharin 1x $>$ 2x $>$ 5x), as well as following aversive taste memory recall (CTA Retrieval), compared with both appetitive learning (Extended Data

Fig. 1-2*B*; Saccharin 1x, Mann–Whitney test: $p < 0.0001$; Sum of ranks: 407, 188; Mann–Whitney $U = 35$) and re-learning (Extended Data Fig. 1-2*B*; Extinction, Mann–Whitney test: $p = 0.0007$; Sum of ranks: 182, 224; Mann–Whitney $U = 29$). However, our comparison failed to account for the influence of complex experiences over time, as differences between Extinction and Re-instatement failed to reach significance (Extended Data Fig. 1-2*B*; Mann–Whitney test: $p = 0.3870$, Sum of ranks: 133.5, 97.50, Mann–Whitney $U = 42.50$), while perplexingly, the ratio of BS:RS aIC-BLA neurons in these groups was differentially increased compared with Saccharin 5x (Extended Data Fig. 1-2*B*; Extinction, Mann–Whitney test: $p = 0.0300$; Sum of ranks: 81, 150; Mann–Whitney $U = 26$; Reinstatement, Mann–Whitney test: $p = 0.3498$; Sum of ranks: 90, 120; Mann–Whitney $U = 35$), but not Saccharin 2x (Extended Data Fig. 1-2*B*; Extinction, Mann–Whitney test: $p = 0.2397$; Sum of ranks: 143.5, 156.5; Mann–Whitney $U = 52.50$; Reinstatement, Mann–Whitney test: $p > 0.9999$; Sum of ranks: 153.50, 122.5; Mann–Whitney $U = 62.50$). No further statistical analyses were performed in intrinsic properties of aIC-BLA regular spiking neurons representing (Figs. 1, 3), because of the small sample size.

Changes in the intrinsic properties of neuronal ensembles have recently been suggested to contribute to homeostatic mechanisms integrating both cellular and synaptic information (C.H. Wu et al., 2021). In our current study, we randomly sampled from neuroanatomically defined LIV–VI aIC-BLA projecting neurons, and even following spike sorting (Extended Data Fig. 1-2), the probability of recording from engram cells (10% of neurons within a region) would be extremely low (Tonegawa et al., 2015). Importantly, the correlative nature does not exclude the possibility that these changes are the consequence of representational drift (Driscoll et al., 2017). We thus set out to examine the hypothesis that applying linear dimension reduction method on the complement of intrinsic properties recorded in BS LIV–VI aIC-BLA neurons would allow us to distinguish between taste experiences that differ in terms of their perceived predictability (or the associated probability for further aversive learning).

Principal component analysis of the profile of intrinsic properties in BS LIV–VI aIC-BLA projecting neurons separates treatment groups in relation to the perceived predictability of taste valence for saccharin

We assigned six of our treatment groups into highly predictive scenarios (Saccharin 5x, CTA Retrieval and Reinstatement), and low predictive scenarios (Saccharin 1x, Saccharin 2x, Extinction). We used parallel analysis to select the components across the complement of intrinsic properties in each treatment group, with the first three principal components (PC1–3) explaining 30.84%, 17.88%, and 13.75% of the total variance, respectively, and 62.47% of the variance, collectively (Extended Data Fig. 5-2). PC1 (Fig. 5*B*; Extended Data Fig. 5-2) was characterized by strong negative loadings for Rheobase (−0.88304), sAHP (−0.85985), and mAHP (−0.82421), while a positive correlation was identified for IR (0.694764). The direction of PC2 (Fig. 5*B*; Extended Data Fig. 5-2) was positively correlated with fAHP (0.682681) and AP halfwidth (0.614103) and was negatively correlated with Excitability at 350 pA (−0.69 587). PC3 (Fig. 5*B*; Extended Data Fig. 5-2) positively correlated with SAG ratio (0.889949) and RMP (0.682681), whereas a significant negative correlation with mAHP (−0.6095) was also identified. Unlike aversive or appetitive taste memory retrieval (i.e., highly predictive), appetitive novelty or extinction learning (i.e., low predictive), was associated with increased input resistance, faster action potential generation and decreased afterhyperpolarization on BS aIC-BLA neurons (Fig. 5). Importantly, PCA of the intrinsic properties of LIV–VI aIC-BLA projecting neurons regardless of cell type (BS and RS together; Extended Data Fig. 5-1), failed to segregate the two groups of treatments. This cell-type-specific profile of intrinsic properties could provide the framework through which BS LIV–VI aIC-BLA projecting neurons are able to inspect the gastrointestinal consequences associated with tastants over prolonged timescales, when these consequences are not accurately predicted by sensory experience or memory retrieval alone (Adaikkan and Rosenblum, 2015; Lavi et al., 2018; Kayyal et al., 2019).

Discussion

Learning and memory are subserved by plasticity in both synapse strength and neuronal intrinsic properties (Citri and Malenka, 2008; Sehgal et al., 2013). While Hebbian rules can explain associative learning paradigms where seconds separate the CS and US (Krabbe et al., 2018), additional cellular-level mechanisms are needed to explain how learning operates in paradigms where the time between CS and US extends to hours (Adaikkan and Rosenblum, 2015; C.H. Wu et al., 2021). In this study, we demonstrate that following taste experiences, taste percept and prior experience are integrated in the intrinsic properties of the aIC in a time-dependent and cell type-specific manner. We further show that regardless of the identity or prior history associated with taste, the intrinsic properties of BS LIV–VI aIC-BLA projecting neurons encodes the perceived confidence of taste valence attribution.

We focused on the aIC-BLA projection; a circuit causally involved in the acquisition and retrieval of CTA memories (Kayyal et al., 2019, 2021). We examined the hypothesis that excitability in aIC-BLA neurons can serve as a taste valence updating mechanism enabling the prolonged ISI between CS and US in CTA learning (Adaikkan and Rosenblum, 2015), and/or contributes to anticipatory valence attribution (Barrett and Simmons, 2015). Our basic proposition diverged from Hebb's famous postulate that cells with increased excitability over hours can potentially wire together with cells conveying incoming modified valence information (Hebb, 1961).

The confidence with which taste valence is encoded is the product of the subjectively perceived (1) appetitive or aversive nature of tastants and (2) novelty or familiarity associated with tastants (Russell, 1980; Kahnt and Tobler, 2017). We first examined each axis separately and later in tandem as to better simulate real-life scenarios. We measured the intrinsic properties of aIC-BLA neurons 1 h

following taste experience, a previously established suitable time point (Jones et al., 1999; Haley et al., 2020).

To dissociate novelty-related changes from those involving hydration, taste identity and familiarity; we compared the intrinsic properties of aIC-BLA neurons following Water, a neutral and familiar tastant, Saccharin, an innately appetitive tastant, in the context of novelty (1×) or familiarity (5×), and Quinine, an innately aversive novel tastant (Fig. 1). Excitability was high following novel saccharin exposure, but not in response to Quinine (Fig. 1*D*). Indeed, concerted activity at the aIC and BLA encodes the presence, identity, and palatability of taste experiences within the 2 s preceding swallowing (Katz et al., 2001; Grossman et al., 2008; Fontanini et al., 2009). Palatability can be enhanced as a function of experience (Austen et al., 2016) but can also be decreased by sensory satiety and alliesthesia (Rolls et al., 1981; Yeomans, 1998; Siemian et al., 2021). However, excitability on the projection was enhanced in response to novelty and was decreased following familiarization (Fig. 1). Further inconsistent with palatability encoding; changes in excitability captured 1 h following novel saccharin exposure subsided 4 h later (Fig. 1), while excitability remained plastic even following longer periods of water restriction, that could be considered monotonous (Fig. 5). Deciphering whether and how aIC-BLA neurons contribute to palatability processing would require *in vivo* recordings to capture taste-evoked changes, within timescales that are beyond the scope and means of our current study (Vincis and Fontanini, 2016).

The correlation identified between excitability and innate current taste valence, encouraged us to examine the predictability of future outcomes following aversive taste memory retrieval. Bearing in mind our previous findings using transcription-dependent activity markers at the aIC (Yiannakas et al., 2021), we hypothesized that aversive taste memory retrieval (CTA Retrieval or Reinstatement) would be associated with decreased excitability compared with stimulus-matched and familiarity-matched controls (Saccharin 2x and Extinction). Indeed, excitability on aIC-BLA projecting neurons following CTA Retrieval was decreased compared with Saccharin 2x (Fig. 2*B*), while Reinstatement was also associated with decreased excitability compared with Extinction (Fig. 3*E*). Hence, regardless of the complexity of taste memory retrieval, excitability in aIC-BLA neurons was best predicted by the subjective predictability of taste valence, increasing in response to innately appetitive taste experiences in which the perceived possibility for avoidance learning was high/taste valence predictability was low (Fig. 4). Conversely, when the subjective confidence with which taste valence was predicted was high, excitability on the projection remained unchanged (Figs. 1, 4).

Innately and learned aversive tastants were both associated with decreased excitability on aIC-BLA projecting neurons compared with appetitive controls; however, these effects were mediated through alternative mechanisms (Figs. 2-4). Quinine increased fAHP on the projection compared with saccharin, regardless of familiarity or perceived valence (Figs. 1, 4). Postspike afterhyperpolarization (AHP) has a key function in transducing the summed result of processed synaptic input, directly impacting neuronal excitability in relation to both learning and aging (Oh and Disterhoft, 2020). In pyramidal cells of the hippocampus and cortex, differences in fAHP are mediated by the Ca^{2+}-dependent and voltage-dependent BK currents that promote repolarization at the beginning APs trains (Shao et al., 1999). Interestingly, studies in the prefrontal cortex (PFC), have shown that fear conditioning decreases excitability, whereas extinction training enhances excitability and decreases medium and slow AHP (Santini et al., 2008; Maglio et al., 2021). Chronic ethanol consumption has shown to suppress excitability and to increase AHP in IC neurons (Luo et al., 2021). Conversely, oxytocin-dependent signaling has been shown to promote social affective behaviors, via increases in excitability and decreases in sAHP in IC neurons (Rogers-Carter et al., 2018). Further studies would be necessary to fully address this, but our findings could indicate that enhanced fAHP is induced by innately aversive tastants or quinine specifically.

Unlike Quinine, CTA memory retrieval was associated with increased AP amplitude and SAG ratio, as well as decreased IR in BS LIV–VI aIC-BLA projecting neurons, compared with control animals (Fig. 2; Extended Data Fig. 2-1). On the other hand, the decreased excitability in the Reinstatement group compared with Extinction was characterized by decreased AP threshold, increased τ, and decreased sAHP (Figs. 3, 4; Extended Data Fig. 3-1). The hyperpolarization-activated, cyclic nucleotide-gated current (I_h) regulates membrane depolarization following hyperpolarization (Hogan and Poroli, 2008; Shah, 2014). The opening of HCN channels generates an inward current, that modulates AHP, RMP and IR in cortical pyramidal and PV interneurons (Yang et al., 2018). However, conductance through I_h channels, regulates synaptic integration at the soma of pyramidal neurons, by suppressing excitability, decreasing IR, and increasing τ (Hogan and Poroli, 2008). Evidence indicates that this dichotomous impact of HCN channels on neuronal excitability, is mediated by A-type K channels at the dendrites (Mishra and Narayanan, 2015), and M-type channels at the soma (Hu et al., 2007). Notably, AP half-width was significantly increased in the Extinction and Reinstatement groups that had undergone extinction training, compared with all other saccharin-treated groups (Fig. 4*F*). Mechanistically, this effect could reflect changes in the distribution and/or the properties of voltage-gated or calcium-gated ion channels (Faber and Sah, 2002; Grubb and Burrone, 2010; Kuba et al., 2010). Such broadening of spike width has also been reported in infralimbic PFC neurons projecting to the amygdala in response to extinction training (Senn et al., 2014). PV-dependent restriction of excitability and burst firing, is instrumental in experience-dependent plasticity in the amygdala (Morrison et al., 2016), the hippocampus (Donato et al., 2013; Xia et al., 2017), and visual cortex (Yazaki-Sugiyama et al., 2009; Kuhlman et al., 2013). Conversely, in the striatum, PV interneurons restrict bursting, calcium influx, and synaptic plasticity to appropriate temporal windows that facilitate learning, but not retrieval (Owen et al., 2018). Elegant recent studies report

that rapid eye movement sleep is associated with a PV-dependent somatodendritic decoupling in pyramidal neurons of the PFC (Aime et al., 2022). At the IC, the maturation of GABAergic PV circuits is key for multisensory integration and pruning of cross-modal input to coordinate the detection of relevant information (Gogolla et al., 2014). Activation of IC PV disrupts the expression of taste-guided goal-directed behavior (Vincis et al., 2020) and enhances taste-guided aversive responses (Yiannakas et al., 2021). Our findings could be indicative of a prediction-dependent decoupling mechanism at the IC, whereby the restriction of bursting activity in LIV–VI aIC-BLA neurons impinges on innate drives toward the tastant and further learning, depending on prior experience.

We further probed our results and hypotheses using PCA and attempted to segregate behaviors based on the perceived ability of the CS to predict the consequences of sensory experience, and the probability for further learning (Fig. 5). We focused on BS LIV–VI aIC-BLA projecting neurons since bursting has been implicated in coincidence detection by deep-layer neurons (Boudewijns et al., 2013; Shai et al., 2015), as well as the encoding of novelty and valence relating to different modalities (Song et al., 2015; Dunn et al., 2018; Yousuf et al., 2019). Our PCA of intrinsic properties in BS LVI-VI aIC-BLA projecting neurons demonstrated that distinct plasticity rules are at play depending on the balance between the probability for associative learning and the certainty with which taste predicts the valence of experience during retrieval (Extended Data Figs. 5-1, 5-2). We propose that increased excitability and reduced fAHP on BS LIV–VI aIC-BLA projecting neurons might represent a transient neuronal state in the absence of adequate predictive cues for the outcome of taste experiences (Adaikkan and Rosenblum, 2015).

The IC has long been considered crucial for interoception, which is increasingly understood to be supported by distinct direct or indirect functional bidirectional connectivity. Indeed, interoceptive inputs relating to the processing, or anticipation of physiological states of hydration and satiety manifest at the pIC (Livneh et al., 2017, 2020; Livneh and Andermann, 2021). However, this is rarely the case when it comes to physiological hydration or satiety inputs and the aIC, that has is primarily involved in interoceptive processes in the context food poisoning or CTA (Chen et al., 2020; Y. Wu et al., 2020). As other studies currently in press demonstrate, hydration correlates and requires decreased activity in aIC-BLA and increases in pIC-BLA CB1 receptor-expressing neurons (Zhao et al., 2022). In fact, and in further accord with our previous findings (Lavi et al., 2018; Kayyal et al., 2019), optogenetic activation of the aIC-BLA projection was found to be anxiogenic, while physiological conditions that are associated with negative valence and anxiety were encoded by changes in activity on the projection (Nicolas et al., 2022). Under uncertain conditions that are associated with greater potential significance, recruitment of the aIC is thought to contribute to attention, effort, and accurate processing (Lovero et al., 2009), as to identify better response options (Preuschoff et al., 2008). In agreement with earlier computational models of the cortical connectivity (Mumford, 1991, 1992), recent work indicates that the aIC facilitates prediction-related encoding driven by hedonics, rather than homeostatic needs (Darevsky et al., 2019; Price et al., 2019; Darevsky and Hopf, 2020). Our results, propose a cellular framework for such an emotional predictive function at the aIC. Indeed, sex can be an important biological variable when examining brain circuits in relation to behavior (Rogers-Carter et al., 2018). Although we cannot exclude the possibility of sex-specific differences, in previous studies where we manipulated activity at the IC in a cell type-specific manner, we found no differences between male and female mice (Kayyal et al., 2019; Yiannakas et al., 2021). Future studies will further explore whether and how the interplay between such distinct mechanisms at the aIC, enables its complex role in learning, memory, and decision-making.

References

Adaikkan C, Rosenblum K (2015) A molecular mechanism underlying gustatory memory trace for an association in the insular cortex. Elife 4:e07582.

Aime M, Calcini N, Borsa M, Campelo T, Rusterholz T, Sattin A, Fellin T, Adamantidis A (2022) Paradoxical somatodendritic decoupling supports cortical plasticity during REM sleep. Science 376:724–730.

Andrade R, Foehring RC, Tzingounis AV (2012) The calcium-activated slow AHP: cutting through the Gordian Knot. Front Cell Neurosci 6:47.

Arieli E, Gerbi R, Shein-Idelson M, Moran A (2020) Temporally-precise basolateral amygdala activation is required for the formation of taste memories in gustatory cortex. J Physiol 598:5505–5522.

Austen JM, Strickland JA, Sanderson DJ (2016) Memory-dependent effects on palatability in mice. Physiol Behav 167:92–99.

Bachmanov AA, Reed DR, Tordoff MG, Price RA, Beauchamp GK (1996) Intake of ethanol, sodium chloride, sucrose, citric acid, and quinine hydrochloride solutions by mice: a genetic analysis. Behav Genet 26:563–573.

Bales MB, Schier LA, Blonde GD, Spector AC (2015) Extensive gustatory cortex lesions significantly impair taste sensitivity to KCl and quinine but not to sucrose in rats. PLoS One 10:e0143419.

Barot SK, Kyono Y, Clark EW, Bernstein IL (2008) Visualizing stimulus convergence in amygdala neurons during associative learning. Proc Natl Acad Sci U S A 105:20959–20963.

Barrett LF, Simmons WK (2015) Interoceptive predictions in the brain. Nat Rev Neurosci 16:419–429.

Bekisz M, Garkun Y, Wabno J, Hess G, Wrobel A, Kossut M (2010) Increased excitability of cortical neurons induced by associative learning: an ex vivo study. Eur J Neurosci 32:1715–1725.

Berman DE (2003) Modulation of taste-induced Elk-1 activation by identified neurotransmitter systems in the insular cortex of the behaving rat. Neurobiol Learn Mem 79:122–126.

Boudewijns ZSRM, Groen MR, Lodder B, Mcmaster MTB, Kalogreades L, De Haan R, Narayanan RT, Meredith RM, Mansvelder HD, de Kock CPJ (2013) Layer-specific high-frequency spiking in the prefrontal cortex of awake rats. Front Cell Neurosci 7:99.

Bures J, Bermudez-Rattoni F, Yamamoto T (1998) The CTA paradigm. In: Conditioned taste aversion: memory of a special kind. Oxford: Oxford University Press.

Chakraborty D, Fedorova O. v, Bagrov AY, Kaphzan H (2017) Selective ligands for Na+/K+-ATPase α isoforms differentially and cooperatively regulate excitability of pyramidal neurons in distinct brain regions. Neuropharmacology 117:338–351.

Chen K, Kogan J, Fontanini A (2020) Spatially distributed representation of taste quality in the gustatory insular cortex of awake behaving mice. Curr Biol 3:1–10.

Chinnakkaruppan A, Wintzer ME, McHugh TJ, Rosenblum K (2014) Differential contribution of hippocampal subfields to components of associative taste learning. J Neurosci 34:11007–11015.
Citri A, Malenka RC (2008) Synaptic plasticity: multiple forms, functions, and mechanisms. Neuropsychopharmacology 33:18–41.
Connors BW, Gutnick MJ, Prince DA (1982) Electrophysiological properties of neocortical neurons in vitro. J Neurophysiol 48:1302–1320.
Darevsky D, Hopf FW (2020) Behavioral indicators of succeeding and failing under higher-challenge compulsion-like alcohol drinking in rat. Behav Brain Res 393:112768.
Darevsky D, Gill TM, Vitale KR, Hu B, Wegner SA, Hopf FW (2019) Drinking despite adversity: behavioral evidence for a head down and push strategy of conflict-resistant alcohol drinking in rats. Addict Biol 24:426–437.
Disterhoft JF, Wu WW, Ohno M (2004) Biophysical alterations of hippocampal pyramidal neurons in learning, ageing and Alzheimer's disease. Ageing Res Rev 3:383–406.
Donato F, Rompani SB, Caroni P (2013) Parvalbumin-expressing basket-cell network plasticity induced by experience regulates adult learning. Nature 504:272–276.
Dunn AR, Kaczorowski CC (2019) Regulation of intrinsic excitability: roles for learning and memory, aging and Alzheimer's disease, and genetic diversity. Neurobiol Learn Mem 164:107069.
Dunn AR, Neuner SM, Ding S, Hope KA, O'Connell KMS, Kaczorowski CC (2018) Cell-type-specific changes in intrinsic excitability in the subiculum following learning and exposure to novel environmental contexts. eNeuro 5:ENEURO.0484-18.2018.
Escobar ML, Bermúdez-Rattoni F (2000) Long-term potentiation in the insular cortex enhances conditioned taste aversion retention. Brain Res 852:208–212.
Faber ESL, Sah P (2002) Physiological role of calcium-activated potassium currents in the rat lateral amygdala. J Neurosci 22:1618–1628.
Fontanini A, Grossman SE, Figueroa JA, Katz DB (2009) Distinct subtypes of basolateral amygdala taste neurons reflect palatability and reward. J Neurosci 29:2486–2495.
Galliano E, Hahn C, Browne LP, Villamayor PR, Tufo C, Crespo A, Grubb MS (2021) Brief sensory deprivation triggers cell type-specific structural and functional plasticity in olfactory bulb neurons. J Neurosci 41:2135–2151.
Garcia J, Kimeldorf DJ, Koelling RA (1955) Conditioned aversion to saccharin resulting from exposure to gamma radiation. Science 122:157–158.
Gogolla N, Takesian AE, Feng G, Fagiolini M, Hensch TK (2014) Sensory integration in mouse insular cortex reflects GABA circuit maturation. Neuron 83:894–905.
Gould NL, Kolatt CS, Kayyal H, Edry E, Rosenblum K (2021) Somatostatin interneurons of the insula mediate QR2 dependent novel taste memory enhancement. eNeuro 8:ENEURO.0152-21.2021.
Graves AR, Moore SJ, Bloss EB, Mensh BD, Kath WL, Spruston N (2012) Hippocampal pyramidal neurons comprise two distinct cell types that are countermodulated by metabotropic receptors. Neuron 76:776–789.
Graves AR, Moore SJ, Spruston N, Tryba AK, Kaczorowski CC (2016) Brain-derived neurotrophic factor differentially modulates excitability of two classes of hippocampal output neurons. J Neurophysiol 116:466–471.
Greenhill SD, Ranson A, Fox K (2015) Hebbian and homeostatic plasticity mechanisms in regular spiking and intrinsic bursting cells of cortical layer 5. Neuron 88:539–552.
Grossman SE, Fontanini A, Wieskopf JS, Katz DB (2008) Learning-related plasticity of temporal coding in simultaneously recorded amygdala-cortical ensembles. J Neurosci 28:2864–2873.
Grubb MS, Burrone J (2010) Activity-dependent relocation of the axon initial segment fine-tunes neuronal excitability. Nature 465:1070–1074.
Hadamitzky M, Bösche K, Engler A, Schedlowski M, Engler H (2015) Extinction of conditioned taste aversion is related to the aversion strength and associated with c-fos expression in the insular cortex. Neuroscience 303:34–41.
Haley MS, Maffei A (2018) Versatility and flexibility of cortical circuits. Neuroscientist 24:456–470.
Haley MS, Fontanini A, Maffei A (2016) Laminar- and target-specific amygdalar inputs in rat primary gustatory cortex. J Neurosci 36:2623–2637.
Haley MS, Bruno S, Fontanini A, Maffei A (2020) LTD at amygdalo-cortical synapses as a novel mechanism for hedonic learning. Elife 9:e55175.
Hanamori T, Kunitake T, Kato K, Kannan H (1998) Responses of neurons in the insular cortex to gustatory, visceral, and nociceptive stimuli in rats. J Neurophysiol 79:2535–2545.
Hebb DO (1961) Distinctive features of learning in the higher animal. Brain mechanisms and learning. A symposium, pp 37–46. Franklin Classics, October 14, 2018.
Hogan QH, Poroli M (2008) Hyperpolarization-activated current (Ih) contributes to excitability of primary sensory neurons in rats. Brain Res 1207:102–110.
Hu H, Vervaeke K, Storm JF (2007) M-channels (Kv7/KCNQ channels) that regulate synaptic integration, excitability, and spike pattern of CA1 pyramidal cells are located in the perisomatic region. J Neurosci 27:1853–1867.
Jarsky T, Mady R, Kennedy B, Spruston N (2008) Distribution of bursting neurons in the CA1 region and the subiculum of the rat hippocampus. J Comp Neurol 506:535–547.
Jones MW, French PJ, Bliss TV, Rosenblum K (1999) Molecular mechanisms of long-term potentiation in the insular cortex in vivo. J Neurosci 19:RC36.
Juárez-Muñoz Y, Ramos-Languren LE, Escobar ML (2017) CaMKII requirement for in vivo insular cortex LTP maintenance and CTA memory persistence. Front Pharmacol 8:822.
Kahnt T, Tobler PN (2017) Reward, value, and salience. In: Decision neuroscience: an integrative perspective, pp 109–120. San Diego: Elsevier.
Kaphzan H, Buffington SA, Ramaraj AB, Lingrel JB, Rasband MN, Santini E, Klann E (2013) Genetic reduction of the α1 Subunit of Na/K-ATPase corrects multiple hippocampal phenotypes in Angelman syndrome. Cell Rep 4:405–412.
Kargl D, Kaczanowska J, Ulonska S, Groessl F, Piszczek L, Lazovic J, Buehler K, Haubensak W (2020) The amygdala instructs insular feedback for affective learning. Elife 9:e60336.
Katz DB, Simon SA, Nicolelis MA (2001) Dynamic and multimodal responses of gustatory cortical neurons in awake rats. J Neurosci 21:4478–4489.
Kayyal H, Yiannakas A, Kolatt Chandran S, Khamaisy M, Sharma V, Rosenblum K, Kayyal H, Chandran SK, Khamaisy M, Sharma V, Rosenblum K (2019) Activity of insula to basolateral amygdala projecting neurons is necessary and sufficient for taste valence representation. J Neurosci 39:9369–9382.
Kayyal H, Kolatt Chandran S, Yiannakas A, Gould N, Khamaisy M, Rosenblum K (2021) Insula to mPFC reciprocal connectivity differentially underlies novel taste neophobic response and learning. Elife 10:e66686.
Kepecs A, Lisman J (2003) Information encoding and computation with spikes and bursts. Network 14:103–118.
Kim EJ, Juavinett AL, Kyubwa EM, Jacobs MW, Callaway EM (2015) Three types of cortical layer 5 neurons that differ in brain-wide connectivity and function. Neuron 88:1253–1267.
Koren T, Yifa R, Am M, Krot M, Boshnak N, Ben-Shaanan TL, Azulay-Debby H, Zalayat I, Avishai E, Hajjo H, Schiller M, Haykin H, Korin B, Farfara D, Hakim F, Kobiler O, Rosenblum K, Rolls A (2021) Insular cortex neurons encode and retrieve specific immune responses. Cell 184:6211.
Krabbe S, Gründemann J, Lüthi A (2018) Amygdala inhibitory circuits regulate associative fear conditioning. Biol Psychiatry 83:800–809.
Kuba H, Oichi Y, Ohmori H (2010) Presynaptic activity regulates Na+ channel distribution at the axon initial segment. Nature 465:1075–1078.

Kuhlman SJ, Olivas ND, Tring E, Ikrar T, Xu X, Trachtenberg JT (2013) A disinhibitory microcircuit initiates critical-period plasticity in the visual cortex. Nature 501:543–546.
Lavi K, Jacobson GA, Rosenblum K, Lüthi A (2018) Encoding of conditioned taste aversion in cortico-amygdala circuits. Cell Rep 24:278–283.
Levitan D, Liu C, Yang T, Shima Y, Lin JY, Wachutka J, Marrero Y, Ghoddousi RAM, Beltrame E da V, Richter TA, Katz DB, Nelson SB (2020) Deletion of stk11 and fos in mouse bla projection neurons alters intrinsic excitability and impairs formation of long-term aversive memory. Elife 9:e61036.
Lin JY, Amodeo LR, Arthurs J, Reilly S (2012) Taste neophobia and palatability: the pleasure of drinking. Physiol Behav 106:515–519.
Livneh Y, Andermann ML (2021) Cellular activity in insular cortex across seconds to hours: sensations and predictions of bodily states. Neuron 109:3576–3593.
Livneh Y, Ramesh RN, Burgess CR, Levandowski KM, Madara JC, Fenselau H, Goldey GJ, Diaz VE, Jikomes N, Resch JM, Lowell BB, Andermann ML (2017) Homeostatic circuits selectively gate food cue responses in insular cortex. Nature 546:611–616.
Livneh Y, Sugden AU, Madara JC, Essner RA, Flores VI, Sugden LA, Resch JM, Lowell BB, Andermann ML (2020) Estimation of current and future physiological states in insular cortex. Neuron 105: 1094–1111.e10.
Lovero KL, Simmons AN, Aron JL, Paulus MP (2009) Anterior insular cortex anticipates impending stimulus significance. Neuroimage 45:976–983.
Luo YX, Galaj E, Ma YY (2021) Differential alterations of insular cortex excitability after adolescent or adult chronic intermittent ethanol administration in male rats. J Neurosci Res 99:649–661.
MacQueen J (1967) Some methods for classification and analysis of multivariate observations. In: Proceedings of the fifth Berkeley Symposium on Mathematical Statistics and Probability, Vol 5, pp 281–297.
Maffei A, Haley M, Fontanini A (2012) Neural processing of gustatory information in insular circuits. Curr Opin Neurobiol 22:709–716.
Maglio LE, Noriega-Prieto JA, Maroto IB, Martin-Cortecero J, Muñoz-Callejas A, Callejo-Móstoles M, de Sevilla DF (2021) Igf-1 facilitates extinction of conditioned fear. Elife 10:e67267.
Mickley GA, Kenmuir CL, McMullen CA, Snyder A, Yocom AM, Likins-Fowler D, Valentine EL, Weber B, Biada JM (2004) Long-term age-dependent behavioral changes following a single episode of fetal N-methyl-D-aspartate (NMDA) receptor blockade. BMC Pharmacol 4:28–16.
Mishra P, Narayanan R (2015) High-conductance states and A-type K+channels are potential regulators of the conductance-current balance triggered by HCN channels. J Neurophysiol 113:23–43.
Morrison DJ, Rashid AJ, Yiu AP, Yan C, Frankland PW, Josselyn SA (2016) Parvalbumin interneurons constrain the size of the lateral amygdala engram. Neurobiol Learn Mem 135:91–99.
Mumford D (1991) On the computational architecture of the neocortex - I. The role of the thalamo-cortical loop. Biol Cybern 65:135–145.
Mumford D (1992) On the computational architecture of the neocortex - II The role of cortico-cortical loops. Biol Cybern 66:241–251.
Nachman M, Ashe JH (1973) Learned taste aversions in rats as a function of dosage, concentration, and route of administration of LiCl. Physiol Behav 10:73–78.
Nicolas C, Ju A, Wu W, Eldirdiri H, Delcasso S,JD, Supiot L, Fomari C, Verite A, Masson M, Rodriguez-Rozada S, Wiegert SJ, Beyeler A (2022) Linking emotional valence and anxiety in a mouse insula-amygdala circuit. Res Sq Available at: https://www.researchsquare.com/article/rs-964107/v1 (Accessed August 28, 2022).
Oh MM, Disterhoft JF (2020) Learning and aging affect neuronal excitability and learning. Neurobiol Learn Mem 167:107133.
Owen SF, Berke JD, Kreitzer AC (2018) Fast-spiking interneurons supply feedforward control of bursting, calcium, and plasticity for efficient learning. Cell 172:683–695.e15.
Piette CE, Baez-Santiago MA, Reid EE, Katz DB, Moran A (2012) Inactivation of basolateral amygdala specifically eliminates palatability-related information in cortical sensory responses. J Neurosci 32:9981–9991.
Preuschoff K, Quartz SR, Bossaerts P (2008) Human insula activation reflects risk prediction errors as well as risk. J Neurosci 28:2745–2752.
Price AE, Stutz SJ, Hommel JD, Anastasio NC, Cunningham KA (2019) Anterior insula activity regulates the associated behaviors of high fat food binge intake and cue reactivity in male rats. Appetite 133:231–239.
Ranck JB (1973) Studies on single neurons in dorsal hippocampal formation and septum in unrestrained rats. Part I. Behavioral correlates and firing repertoires. Exp Neurol 41:462–531.
Rieger NS, Varela JA, Ng AJ, Granata L, Djerdjaj A, Brenhouse HC, Christianson JP (2022) Insular cortex corticotropin-releasing factor integrates stress signaling with social affective behavior. Neuropsychopharmacology 47:1156–1168.
Rodríguez-Durán LF, Martínez-Moreno A, Escobar ML, Rodriguez-Duran LF, Martinez-Moreno A, Escobar ML (2017) Bidirectional modulation of taste aversion extinction by insular cortex LTP and LTD. Neurobiol Learn Mem 142:85–90.
Rogers-Carter MM, Varela JA, Gribbons KB, Pierce AF, McGoey MT, Ritchey M, Christianson JP (2018) Insular cortex mediates approach and avoidance responses to social affective stimuli. Nat Neurosci 21:404–414.
Rogers-Carter MM, Djerdjaj A, Gribbons KB, Varela JA, Christianson JP (2019) Insular cortex projections to nucleus accumbens core mediate social approach to stressed juvenile rats. J Neurosci 39:8717–8729.
Rolls BJ, Rolls ET, Rowe EA, Sweeney K (1981) Sensory specific satiety in man. Physiol Behav 27:137–142.
Rosenblum K, Berman DE, Hazvi S, Lamprecht R, Dudai Y (1997) NMDA receptor and the tyrosine phosphorylation of its 2B subunit in taste learning in the rat insular cortex. J Neurosci 17:5129–5135.
Russell JA (1980) A circumplex model of affect. J Pers Soc Psychol 39:1161–1178.
Sadacca BF, Rothwax JT, Katz DB (2012) Sodium concentration coding gives way to evaluative coding in cortex and amygdala. J Neurosci 32:9999–10011.
Samengo I, Mato G, Elijah DH, Schreiber S, Montemurro MA (2013) Linking dynamical and functional properties of intrinsically bursting neurons. J Comput Neurosci 35:213–230.
Santini E, Quirk GJ, Porter JT (2008) Fear conditioning and extinction differentially modify the intrinsic excitability of infralimbic neurons. J Neurosci 28:4028–4036.
Schachtman TR, Brown AM, Miller RR (1985) Reinstatement-induced recovery of a taste-LiCl association following extinction. Anim Learn Behav 13:223–227.
Schier LA, Spector AC (2019) The functional and neurobiological properties of bad taste. Physiol Rev 99:605–663.
Sehgal M, Song C, Ehlers VL, Moyer JR (2013) Learning to learn - Intrinsic plasticity as a metaplasticity mechanism for memory formation. Neurobiol Learn Mem 105:186–199.
Senn V, Wolff SBE, Herry C, Grenier F, Ehrlich I, Gründemann J, Fadok JP, Müller C, Letzkus JJ, Lüthi A (2014) Long-range connectivity defines behavioral specificity of amygdala neurons. Neuron 81:428–437.
Shah MM (2014) Cortical HCN channels: function, trafficking and plasticity. J Physiol 592:2711–2719.
Shai AS, Anastassiou CA, Larkum ME, Koch C (2015) Physiology of layer 5 pyramidal neurons in mouse primary visual cortex: coincidence detection through bursting. PLoS Comput Biol 11:e1004090.
Shao LR, Halvorsrud R, Borg-Graham L, Storm JF (1999) The role of BK-type Ca2+-dependent K+ channels in spike broadening during repetitive firing in rat hippocampal pyramidal cells. J Physiol 521:135–146.
Sharma V, Ounallah-Saad H, Chakraborty D, Hleihil M, Sood R, Barrera I, Edry E, Kolatt Chandran S, ben Tabou de Leon S, Kaphzan H, Rosenblum K (2018) Local inhibition of PERK enhances memory and reverses age-related deterioration of cognitive and neuronal properties. J Neurosci 38:648–658.

Shor OL, Fidzinski P, Behr J (2009) Muscarinic acetylcholine receptors and voltage-gated calcium channels contribute to bidirectional synaptic plasticity at CA1-subiculum synapses. Neurosci Lett 449:220–223.

Siemian JN, Arenivar MA, Sarsfield S, Aponte Y (2021) Hypothalamic control of interoceptive hunger. Curr Biol 31:3797–3809.e5.

Slouzkey I, Maroun M (2016) PI3-kinase cascade has a differential role in acquisition and extinction of conditioned fear memory in juvenile and adult rats. Learn Mem 23:723–731.

Song C, Moyer JR (2018) Layer- and subregion-specific differences in the neurophysiological properties of rat medial prefrontal cortex pyramidal neurons. J Neurophysiol 119:177–191.

Song C, Detert JA, Sehgal M, Moyer JR (2012) Trace fear conditioning enhances synaptic and intrinsic plasticity in rat hippocampus. J Neurophysiol 107:3397–3408.

Song C, Ehlers VL, Moyer JR (2015) Trace fear conditioning differentially modulates intrinsic excitability of medial prefrontal cortex–basolateral complex of amygdala projection neurons in infralimbic and prelimbic cortices. J Neurosci 35:13511–13524.

Soto A, Gasalla P, Begega A, López M (2017) c-Fos activity in the insular cortex, nucleus accumbens and basolateral amygdala following the intraperitoneal injection of saccharin and lithium chloride. Neurosci Lett 647:32–37.

Staff NP, Jung HY, Thiagarajan T, Yao M, Spruston N (2000) Resting and active properties of pyramidal neurons in subiculum and CA1 of rat hippocampus. J Neurophysiol 84:2398–2408.

Stone ME, Fontanini A, Maffei A (2020) Synaptic integration of thalamic and limbic inputs in rodent gustatory cortex. eNeuro 7: ENEURO.0199-19.2019.

Suzuki A, Josselyn SA, Frankland PW, Masushige S, Silva AJ, Kida S (2004) Memory reconsolidation and extinction have distinct temporal and biochemical signatures. J Neurosci 24:4787–4795.

Turrigiano G (2011) Too many cooks? Intrinsic and synaptic homeostatic mechanisms in cortical circuit refinement. Annu Rev Neurosci 34:89–103.

Ventura R, Morrone C, Puglisi-Allegra S (2007) Prefrontal/accumbal catecholamine system determines motivational salience attribution to both reward-and aversion-related stimuli. Proc Natl Acad Sci U S A 104:5181–5186.

Vincis R, Fontanini A (2016) A gustocentric perspective to understanding primary sensory cortices. Curr Opin Neurobiol 40:118–124.

Vincis R, Chen K, Czarnecki L, Chen J, Fontanini A (2020) Dynamic representation of taste-related decisions in the gustatory insular cortex of mice. Curr Biol 30:1834–1844.e5.

Wang L, Gillis-Smith S, Peng Y, Zhang J, Chen X, Salzman CD, Ryba NJP, Zuker CS (2018) The coding of valence and identity in the mammalian taste system. Nature 558 558:127–131.

Wozny C, Maier N, Schmitz D, Behr J (2008) Two different forms of long-term potentiation at CA1-subiculum synapses. J Physiol 586:2725–2734.

Wu CH, Ramos R, Katz DB, Turrigiano GG (2021) Homeostatic synaptic scaling establishes the specificity of an associative memory. Curr Biol 31:2274–2285.e5.

Wu Y, Chen C, Chen M, Qian K, Lv X, Wang H, Jian L, Yu L, Zhu M, Qiu S (2020) The anterior insular cortex unilaterally controls feeding in response to aversive visceral stimuli in mice. Nat Commun 11:640.

Xia F, Richards BA, Tran MM, Josselyn SA, Takehara-Nishiuchi K, Frankland PW, Bartos M (2017) Parvalbumin-positive interneurons mediate neocortical-hippocampal interactions that are necessary for memory consolidation. Elife 6:e27868.

Yang SS, Li YC, Coley AA, Chamberlin LA, Yu P, Gao WJ (2018) Cell-type specific development of the hyperpolarization-activated current, Ih, in prefrontal cortical neurons. Front Synaptic Neurosci 10:7.

Yazaki-Sugiyama Y, Kang S, Câteau H, Fukai T, Hensch TK (2009) Bidirectional plasticity in fast-spiking GABA circuits by visual experience. Nature 462:218–221.

Yeomans MR (1998) Taste, palatability and the control of appetite. Proc Nutr Soc 57:609–615.

Yiannakas A, Kolatt Chandran S, Kayyal H, Gould N, Khamaisy M, Rosenblum K (2021) Parvalbumin interneuron inhibition onto anterior insula neurons projecting to the basolateral amygdala drives aversive taste memory retrieval. Curr Biol 31:2770–2784.e6.

Yousuf H, Ehlers VL, Sehgal M, Song C, Moyer JR (2019) Modulation of intrinsic excitability as a function of learning within the fear conditioning circuit. Neurobiol Learn Mem 167:107132.

Zeldenrust F, Wadman WJ, Englitz B (2018) Neural coding with bursts—Current state and future perspectives. Front Comput Neurosci 12:48.

Zhao Z, Covelo A, Mitra A, Varilh M, Wu Y, Jacky D, Cannich A, Bellocchio L, Marsicano G, Beyeler A (2022) Cannabinoids regulate an insula circuit controlling water intake. bioRxiv 484736. https://doi.org/10.1101/2022.03.18.484736.